University of the Pacific
Scholarly Commons

All Dugoni School of Dentistry Faculty Articles | All Faculty Scholarship

4-1-2017

Gpr124 is essential for blood-brain barrier integrity in central nervous system disease

Junlei Chang
Stanford University School of Medicine

Michael R. Mancuso
Stanford University School of Medicine

Carolina Maier
Stanford University School of Medicine

Xibin Liang
Stanford University School of Medicine

Kanako Yuki
Stanford University School of Medicine

See next page for additional authors

Follow this and additional works at: https://scholarlycommons.pacific.edu/dugoni-facarticles

 Part of the Medicine and Health Sciences Commons

Recommended Citation

Chang, J., Mancuso, M. R., Maier, C., Liang, X., Yuki, K., Yang, L., Kwong, J. W., Wang, J., Rao, V., Vallon, M., Kosinski, C., Zhang, J. J., Mah, A. T., Xu, L., Li, L., Gholamin, S., Reyes, T. F., Li, R., Kuhnert, F., Han, X., Yuan, J., Chiou, S., Brettman, A. D., Daly, L., Corney, D. C., Cheshier, S. H., Shortliffe, L. D., Wu, X., & Snyder, M. (2017). Gpr124 is essential for blood-brain barrier integrity in central nervous system disease. *Nature Medicine, 23*(4), 450–460. DOI: 10.1038/nm.4309
https://scholarlycommons.pacific.edu/dugoni-facarticles/721

This Article is brought to you for free and open access by the All Faculty Scholarship at Scholarly Commons. It has been accepted for inclusion in All Dugoni School of Dentistry Faculty Articles by an authorized administrator of Scholarly Commons. For more information, please contact mgibney@pacific.edu.

Authors

Junlei Chang, Michael R. Mancuso, Carolina Maier, Xibin Liang, Kanako Yuki, Lu Yang, Jeffrey W. Kwong, Jing Wang, Varsha Rao, Mario Vallon, Cynthia Kosinski, J. J. Haijing Zhang, Amanda T. Mah, Lijun Xu, Le Li, Sharareh Gholamin, Teresa F. Reyes, Rui Li, Frank Kuhnert, Xiaoyuan Han, Jenny Yuan, Shin Heng Chiou, Ari D. Brettman, Lauren Daly, David C. Corney, Samuel H. Cheshier, Linda D. Shortliffe, Xiwei Wu, and Michael Snyder

This article is available at Scholarly Commons: https://scholarlycommons.pacific.edu/dugoni-facarticles/721

Author Manuscript

Author Manuscript

Author Manuscript

Author Manuscript

HHS Public Access

Author manuscript

Nat Med. Author manuscript; available in PMC 2017 August 17.

Published in final edited form as:

Nat Med. 2017 April ; 23(4): 450–460. doi:10.1038/nm.4309.

Gpr124 is essential for blood–brain barrier integrity in central nervous system disease

Junlei Chang[1,10,11], **Michael R Mancuso**[1,11], **Carolina Maier**[2], **Xibin Liang**[3], **Kanako Yuki**[1], **Lu Yang**[4], **Jeffrey W Kwong**[1], **Jing Wang**[3], **Varsha Rao**[5], **Mario Vallon**[1], **Cynthia Kosinski**[1], **J J Hailing Zhang**[1], **Amanda T Mah**[1], **Lijun Xu**[6], **Le Li**[6], **Sharareh Gholamin**[2], **Teresa F Reyes**[1], **Rui Li**[7], **Frank Kuhnert**[1], **Xiaoyuan Han**[8], **Jenny Yuan**[1], **Shin-Heng Chiou**[5], **Ari D Brettman**[1], **Lauren Daly**[1], **David C Corney**[1], **Samuel H Cheshier**[2], **Linda D Shortliffe**[8], **Xiwei Wu**[4], **Michael Snyder**[5], **Pak Chan**[2], **Rona G Giffard**[6], **Howard Y Chang**[7,9], **Katrin Andreasson**[3], and **Calvin J Kuo**[1]

[1]Department of Medicine, Stanford University School of Medicine, Stanford, California, USA

[2]Department of Neurosurgery, Stanford University School of Medicine, Stanford, California, USA

[3]Department of Neurology and Neurological Sciences, Stanford University School of Medicine, Stanford, California, USA

[4]Department of Molecular and Cellular Biology and Integrative Genomics Core, City of Hope, Duarte, California, USA

[5]Department of Genetics, Stanford University School of Medicine, Stanford, California, USA

[6]Department of Anesthesiology, Perioperative and Pain Medicine, Stanford University School of Medicine, Stanford, California, USA

[7]Department of Dermatology, Stanford University School of Medicine, Stanford, California, USA

[8]Department of Urology, Stanford University School of Medicine, Stanford, California, USA

[9]Center for Personal Dynamic Regulomes, Stanford University School of Medicine, Stanford, California, USA

Abstract

Although blood–brain barrier (BBB) compromise is central to the etiology of diverse central nervous system (CNS) disorders, endothelial receptor proteins that control BBB function are

Reprints and permissions information is available online at http://www.nature.com/reprints/index.html.

Correspondence should be addressed to C.J.K. (cjkuo@stanford.edu).

[10]Present address: Center for Antibody Drug, Institute of Biomedicine and Biotechnology, Shenzhen Institutes of Advanced Technology, Chinese Academy of Sciences, Shenzhen, China.

[11]These authors contributed equally to this work.

AUTHOR CONTRIBUTIONS

J.C. and M.R.M. designed and performed experiments, analyzed the data and wrote the manuscript. C.M., X.L., K. Y., L.X., L.L. and J.W. performed the tMCAO and tumor cell implantation surgeries, performed experiments and analyzed data. J.W.K, V.R., M.V., C.K., J.H.Z., A.T.M., S.G., T.R., R.L., F.K., X.H., J.Y., S.-H.C., A.D.B., L.D. and D.C.C. performed experiments and analyzed data. L.Y. and X.W. analyzed the RNA-seq data. S.H.C., L.D.S., M.S., P.C., H.Y.C., R.G.G. and K.A. designed experiments and analyzed the data. C.J.K. conceived and supervised the project, designed experiments, interpreted the data and wrote the manuscript.

COMPETING FINANCIAL INTERESTS The authors declare no competing financial interests.

Author Manuscript Author Manuscript Author Manuscript Author Manuscript

poorly defined. The endothelial G-protein-coupled receptor (GPCR) Gpr124 has been reported to be required for normal forebrain angiogenesis and BBB function in mouse embryos, but the role of this receptor in adult animals is unknown. Here *Gpr124* conditional knockout (CKO) in the endothelia of adult mice did not affect homeostatic BBB integrity, but resulted in BBB disruption and microvascular hemorrhage in mouse models of both ischemic stroke and glioblastoma, accompanied by reduced cerebrovascular canonical Wnt–β-catenin signaling. Constitutive activation of Wnt–β-catenin signaling fully corrected the BBB disruption and hemorrhage defects of *Gpr124*-CKO mice, with rescue of the endothelial gene tight junction, pericyte coverage and extracellular-matrix deficits. We thus identify Gpr124 as an endothelial GPCR specifically required for endothelial Wnt signaling and BBB integrity under pathological conditions in adult mice. This finding implicates Gpr124 as a potential therapeutic target for human CNS disorders characterized by BBB disruption.

The integrity of the cerebrovasculature is regulated by a blood–brain barrier (BBB), comprised of cooperating cellular, junctional and transporter elements. As the interface between neural tissue and blood, the BBB protects the brain from toxins and pathogens and facilitates neuronal function[1,2]. BBB disruption is associated with multiple central nervous system (CNS) disorders, including stroke, glioblastoma, Alzheimer's disease and multiple sclerosis, and it contributes to the progression of these disorders[1–3]. Despite the potential benefit that BBB modulation might have in the treatment of CNS pathologies, the identity of endothelial receptors that control adult BBB integrity has remained elusive. It is also uncertain whether distinct mechanisms modulate the adult BBB during homeostasis as compared to disease states.

The barrier function of the brain endothelium in mice develops during angiogenic invasion of the neuroepithelium at embryonic day 9.5 (E9.5). Normal embryonic CNS angiogenesis and BBB formation requires numerous genes, including *Kdr* (also known as *Vegfr2*), *Nrp1, Nrp2*, *Tgfbr1, Tgfbr2*, *Gpr124*, β-catenin (encoded by *Ctnnb1*) and *Mfsd2a* in the endothelium, and *Vegfa*, *Wnt7a*, *Wnt7b*, *Id1*, *Id3* and *Itgav* or *Itgb8* in the neuroepithelium[4–7]. Moreover, the canonical Wnt–β-catenin signaling pathway plays an essential part in embryonic BBB formation; this pathway controls BBB formation via the action of ligands (Wnt7a/7b (refs. 8,9); Norrin[10–12]), receptors (Fzd4 (refs. 10–13)), coreceptors (Lrp5/6 (ref. 14)), coactivators (Tspan12 (ref. 15); Gpr124 (refs. 16–18); Reck[19,20]) and β-catenin itself[8,9,21]. Moreover, the barrier property of the brain endothelium can be induced *in vitro* by Wnt–β-catenin signaling[21–23].

Despite the well-established role of endothelial Wnt signaling in embryonic BBB formation, its contribution to adult BBB function under homeostatic and pathologic conditions remains poorly characterized. During homeostasis, endothelial *Fzd4* deletion produces BBB compromise in adult mice[12], whereas conditional deletion of endothelial *Ctnnb1* in adult mice induces BBB breakdown and brain petechial hemorrhage, either through transcriptional activation or the adherens-junction functions of β-catenin[24]. During pathologic conditions, Wnt–β-catenin signaling in unfractionated brain tissue is correlated with tissue damage and hemorrhagic transformation after ischemic stroke[25,26], and

Author Manuscript Author Manuscript Author Manuscript Author Manuscript

endothelial Wnt–β-catenin signaling is functionally implicated in the regulation of vascular integrity in glioblastoma[27].

We and others have shown that the adhesion GPCR Gpr124 functions cell autonomously in brain endothelium to regulate embryonic forebrain and neural-tube angiogenesis[16–18]. *Gpr124* deletion elicits a pronounced embryonic lethal CNS-specific phenotype characterized by impaired angiogenesis and the presence of hemorrhagic glomeruloid malformations, coupled to developmental BBB defects and loss of expression of glucose transporter 1 (*Glut1*, also known as *Slc2a1*), a BBB marker. In this setting, Gpr124 functions as a Wnt7-specific coactivator of canonical Wnt–β-catenin signaling through undefined direct or indirect mechanisms[20,28,29]. However, the role of Gpr124 in pathologic conditions in the adult is unknown. Here, using adult mice with conditional knockout (CKO) of *Gpr124* in the endothelia, we examined Gpr124 function and the role of downstream canonical Wnt–β-catenin signaling in homeostasis and pathology.

RESULTS

Postnatal or adult *Gpr124* deletion does not affect CNS angiogenesis, BBB development or maintenance

To bypass the embryonic lethality of constitutive *Gpr124* deletion, we created $Gpr124^{flox}$ mice, in which the *Gpr124* mutated allele contains exon 1 flanked by *loxP* sites, in the C57Bl/6J background (Supplementary Fig. 1a,b)[16]. We used $Gpr124^{flox/flox}$;*CMV-Cre* mice to induce global *Gpr124* deletion; in these mice, there was forebrain hemorrhage and embryonic lethality (Supplementary Fig. 1c), which was similar to the phenotype of mice with a $Gpr124^{lacZ}$ knock-in null allele[16]. Next, we generated $Gpr124^{flox/-}$;*ROSA-CreER* mice (global *Gpr124* CKO) to achieve global *Gpr124* deletion upon tamoxifen treatment (Supplementary Fig. 2a,b); $Gpr124^{flox/+}$;*ROSACreER* littermates were used as heterozygous controls (het). Global *Gpr124* deletion, when initiated either at postnatal day 1 or at 2–3 months of age, did not alter CNS vascular patterning, expression of the BBB marker Glut1 or survival over a subsequent 1-year period (Supplementary Figs. 2 and 3), which contrasts with the absolute requirement of *Gpr124* for developmental induction of endothelial Glut1 expression at E12.5 (refs. 16,17). Furthermore, global *Gpr124* deletion, when initiated at 7–8 weeks of age, did not alter BBB permeability to small exogenous tracers, either Sulfo-NHS-biotin (molecular weight (MW) = 443 g/mol) or Evans blue (MW = 961 g/mol) (Supplementary Fig. 4a–d). Taken together, these results indicate that Gpr124 is dispensable for vascular homeostasis and BBB integrity in the adult CNS.

Gpr124 deficiency induces rapid BBB breakdown and hemorrhagic transformation following experimental ischemic stroke

Given that *Gpr124* deletion did not affect homeostatic CNS angiogenesis and BBB function, we next examined pathologic models. During brain ischemia and reperfusion, BBB breakdown underlies the development of edema and hemorrhagic transformation and facilitates reperfusion injury, inflammation and neuronal death[1,30]. We used the transient middle cerebral artery occlusion stroke model (tMCAO), in which cerebral ischemia is followed by reperfusion[31]. We subjected male global *Gpr124*-CKO mice or control global

Author Manuscript Author Manuscript Author Manuscript Author Manuscript

Gpr124-het mice (12–14 weeks of age; mice of this age were used in all subsequent experiments) to 1 h of tMCAO and 1 d of reperfusion. The global *Gpr124*-CKO mice displayed increased BBB breakdown, as compared to control het mice, and rapidly developed parenchymal microvascular hemorrhages in the cortex and striatum of the stroke hemisphere within 24 h after the onset of reperfusion; these hemorrhages became more severe as reperfusion continued and were confined exclusively to infarcted regions. By contrast, hemorrhage in global *Gpr124*-het mice was less prevalent and, when present, was much milder (Fig. 1a,b,d and Supplementary Fig. 5a–c). Accordingly, global *Gpr124*-CKO mice demonstrated a significantly increased neurological score ($P < 0.01$; Supplementary Fig. 6a), reduced survival (Fig. 1f) and increased infarct size (Fig. 1h), as compared to control het mice. The defect in BBB integrity in global *Gpr124*-CKO mice occurred before hemorrhage, because increased leakage of the endogenous plasma protein fibrinogen and of the exogenous tracer Sulfo-NHS-biotin occurred as early as after 1 h after reperfusion, in the absence of erythrocyte extravasation (Fig. 1i,j and Supplementary Fig. 5f). Global *Gpr124*-het mice did not exhibit substantial differences in poststroke hemorrhage when compared to wild-type mice (data not shown), and endothelial *Gpr124* expression was not altered by stroke (Supplementary Fig. 5h).

Given that Gpr124 is expressed by both adult CNS endothelial cells (ECs) and pericytes (PCs)[16], we next investigated whether the loss of Gpr124 expression in endothelial cells is responsible for the hemorrhagic-stroke phenotype in global *Gpr124*-CKO mice. We used an ECspecific *Cdh5-CreER* allele[32], which is highly active in adult brain ECs but not PCs, given that tamoxifen treatment of *Cdh5-CreER;ROSA-loxP*Stop-*loxP-TdTomato* mice (termed *Cdh5-CreER;ROSA-TdTomato* mice) robustly induced endothelial TdTomato expression (~90%; Supplementary Fig. 7a,c). We treated *Gpr124*$^{flox/-}$;*Cdh5-CreER* mice (EC *Gpr124*-CKO) and control heterozygous littermates (*Gpr124*$^{flox/+}$; *Cdh5-CreER*; EC *Gpr124*-het mice) with tamoxifen at 7–8 weeks of age. Tamoxifen-treated EC *Gpr124*-CKO mice exhibited robust reduction of *Gpr124* mRNA levels in fluorescence-activated cell sorting (FACS)-sorted CD31$^+$ ECs (>95%) but not Pdgfr-β$^+$ PCs (~2%) (Supplementary Fig. 7d). After 1 h of tMCAO, male EC *Gpr124*-CKO mice fully recapitulated the rapid BBB breakdown and hemorrhagictransformation phenotype of male global *Gpr124*-CKO mice, with increased Evans blue extravasation as compared to EC *Gpr124*-het mice (Fig. 1c–e; Supplementary Fig. 5d,e). EC-specific *Gpr124*-CKO mice exhibited increased infarct size, reduced survival and worsened neurological scores as compared to control het mice (Fig. 1g,h; Supplementary Fig. 6b). Notably, BBB leak in EC-specific *Gpr124*-CKO mice could be detected by plasma fibrinogen or exogenous biotin extravasation as early as 1 h after reperfusion, clearly preceding the onset of hemorrhage (Fig. 1i,j; Supplementary Fig. 5f,g). Although the outcome of ischemic stroke is sexually dimorphic owing to the effects of sex hormones, as well as other differences[33,34], both female global and EC *Gpr124*-CKO mice showed a hemorrhagicstroke phenotype similar to that of the corresponding male mice (Supplementary Fig. 8). Overall, endothelial *Gpr124* seems to be essential for the maintenance of BBB integrity after the occurrence of acute brain ischemia and reperfusion injury.

Author Manuscript Author Manuscript Author Manuscript Author Manuscript

Wnt–β-catenin signaling is active in adult cerebrovasculature and reduced by *Gpr124* CKO

Because embryonic *Gpr124* deletion induces BBB deficits and lethal brain hemorrhage by decreasing endothelial Wnt–β-catenin signaling[20,28,29], we tested whether Gpr124 similarly used Wnt–β-catenin signaling to regulate adult pathologic BBB function. Using BAT-Gal Wnt-reporter mice, in which β-galactosidase is controlled by a Wnt-responsive promoter[21], vascular Wnt–β-catenin signaling has been shown to be decreased during postnatal and adult life as compared to embryonic CNS angiogenesis[21], although numerous studies suggest that active Wnt–β-catenin signaling occurs in the adult cerebrovasculature[12,14,35,36]. Using RNA-seq analysis, we found abundant expression of essential Wnt–β-catenin signaling components, such as *Fzd4*, *Lrp5*, *Lrp6*, *Ctnnb1*, *Lef1* and *Tcf7*, as well as Wnt target genes, such as *Axin2* and *Apcdd1* (refs. 9,29), in adult brain ECs (Supplementary Fig. 9a and Supplementary Table 1). Moreover, we observed low but detectable adult brain vascular β-galactosidase expression in BAT-Gal mice (Supplementary Fig. 9b). These data collectively indicate the presence of active Wnt–β-catenin signaling in the adult cerebrovasculature.

We next asked whether *Gpr124* CKO reduces Wnt–β-catenin signaling in adult brain ECs. When transduced with Wnt7b adenovirus, primary cultured brain ECs from adult global *Gpr124*-het mice, but not from global *Gpr124*-CKO mice, showed increased expression of the Wnt target genes *Axin2* and *Apcdd1* (Fig. 2a). Freshly isolated ECs sorted by FACS from adult global *Gpr124* CKO showed significantly reduced expression of *Axin2*, *Apcdd1* and *Cldn5* mRNA levels, as compared to that in ECs from adult global het mice (Fig. 2b). Notably, claudin 5 is a major brain endothelial tight-junction protein[35] that is regulated by Wnt signaling in ECs in embryos and in the adult brain[12,28]. Expression of constitutively active β-catenin potently rescued impaired canonical Wnt signaling in ECs of EC *Gpr124*-CKO mice, as assessed by real-time (RT)–qPCR analysis of the Wnt targets *Axin2*, *Apcdd1*, *Prkcb* and *Nkd1* in FACS-sorted brain ECs (Fig. 2c).

To further evaluate the effects of *Gpr124* deletion on Wnt–β-catenin signaling *in vivo*, we performed RNA-seq analysis using $Ctnnb1^{lox(ex3)/+}$ mice. In the $Ctnnb1^{lox(ex3)}$ allele, exon 3 of *Ctnnb1* (encoding β-catenin), which contains the negative-regulatory glycogen synthase kinase-3 phosphorylation sites, is flanked by *loxP* sites; excision upon tamoxifen treatment leads to the expression of a stabilized form of β-catenin protein, which results in constitutive activation of canonical Wnt signaling[37]. Accordingly, tamoxifen treatment of $Ctnnb1^{lox(ex3)/+}$;*Cdh5-CreER* mice (termed β-cat mice) resulted in endothelial-specific Wnt–β-catenin signaling activation. RNA-seq analysis of FACS-purified $CD31^+$ adult brain ECs from β-cat and WT littermate control mice showed that a 12-gene Wnt signature was robustly induced by the activation of endothelial canonical Wnt signaling *in vivo* (Fig. 2d). Moreover, this 12-gene Wnt signature was downregulated in brain ECs of global *Gpr124*-CKO mice below the baseline level in the control het littermates, as assessed by RNA-seq analysis, indicating a reduction of Wnt signaling upon *Gpr124* deletion (Fig. 2d). DAVID pathway analysis of differentially expressed genes[38] revealed that *Gpr124*-CKO and β-catenin activation reciprocally regulated genes important for extracellular matrix (ECM)–receptor interaction and cell–cell–matrix adhesion, angiogenesis and vascular development, and cell growth and death (Supplementary Tables 2 and 3). Thus, *Gpr124* is essential for the maintenance of adult cerebrovascular Wnt–β-catenin signaling.

Author Manuscript Author Manuscript Author Manuscript Author Manuscript

Endothelial-specific, constitutive activation of Wnt–β-catenin signaling improves BBB function and rescues the *Gpr124*-CKO hemorrhagic-stroke phenotype

To test the role of Wnt–β-catenin signaling downstream of Gpr124 in the stroke model, we performed RNA-seq analysis of FACS-sorted brain CD31$^+$ ECs from global *Gpr124*-CKO mice as opposed to het mice, comparing ECs isolated from the stroke- and nonstroke-afflicted hemispheres after 1 h of tMCAO and 1 d of reperfusion. In het mouse brain ECs, the 12-gene Wnt signature was decreased significantly in ECs from the stroke-afflicted, as compared to the nonstroke-afflicted, hemisphere, and the gene signature was further decreased in *Gpr124*-CKO ECs as compared to control het ECs (Fig. 2e). These data suggest that endothelial Wnt signaling is compromised by stroke and further decreased by *Gpr124* deletion after stroke.

To test whether endothelial-specific activation of canonical Wnt signaling could rescue the reduced Wnt signaling and hemorrhagic stroke phenotype of *Gpr124*-CKO mice, we induced endothelial *Gpr124* deletion by tamoxifen with or without endothelial-specific activation of β-catenin. In this experiment, *Gpr124*$^{flox/-}$*;Ctnnb1*$^{lox(ex3)/+}$*;Cdh5-CreER* mice (EC CKO; β-cat) were used for combined endothelial-specific deletion of *Gpr124* and activation of β-catenin, whereas heterozygous *Gpr124*$^{flox/+}$*;Ctnnb1*$^{lox(ex3)/+}$*; Cdh5-CreER* littermates (EC het; β-cat) served as controls. From the same crosses that generated the EC CKO; β-cat mice and EC het; β-cat mice, EC-specific *Gpr124*-CKO mice and *Gpr124*-het mice without β-catenin activation were also generated (EC CKO and EC het, respectively). Endothelial-specific β-catenin activation fully rescued the hemorrhagic stroke phenotype of endothelial *Gpr124*-CKO mice, including profound reduction of poststroke hemorrhage (Fig. 2f), decreased infarct size (Fig. 2g), increased survival (Fig. 2h) and improved BBB function, as assessed by reduced Sulfo-NHS-Biotin and plasma fibrinogen extravasation (Fig. 2i,j). Taken together, these results demonstrate that Gpr124 acts through canonical β-catenin signaling in the adult brain vasculature in stroke.

Gpr124–Wnt signaling regulates endothelial tight junctions, pericytes and extracellular matrix following stroke

To further identify downstream effectors of Gpr124–Wnt signaling following stroke, we examined components of the neurovascular unit— endothelial tight junctions, pericytes and basement membrane—that are essential for BBB integrity[1,7]. Under homeostatic conditions, EC *Gpr124*-CKO mice showed significantly decreased *Cldn5* mRNA and protein levels as compared to het control mice, which were rescued by superimposed constitutive β-catenin activation (Fig. 3a; Supplementary Fig. 10a,b). Moreover, global *Gpr124*-CKO and het mouse brains did not markedly differ in pericyte morphology and coverage or perivascular ECM (laminin and collagen IV) (Supplementary Figs. 10c,d and 11). In contrast to the lack of effects of *Gpr124* deletion under homeostatic conditions, upon 1 h of tMCAO, global *Gpr124*-CKO mice but not het mice exhibited rapid detachment of pericytes from vessels in the infarct region within 1 d (Fig. 3b; Supplementary Fig. 11a,b). Moreover, the detached Pdgfr-β$^+$ or desmin$^+$ pericytes in global *Gpr124*-CKO mice progressively disappeared after 3 to 5 days of reperfusion, whereas in *Gpr124* het mice, the pericyte pool was substantially expanded, as assessed by both IF staining and electron microscopy (Supplementary Fig. 11). Notably, we observed pericyte loss in EC-specific *Gpr124*-CKO mice at day 5 following

Author Manuscript Author Manuscript Author Manuscript Author Manuscript

stroke, and EC-specific constitutive β-catenin expression fully restored poststroke pericyte coverage (Fig. 3c,d).

Pdgfb in endothelial cells and Pdgfr-β in pericytes regulate CNS pericyte coverage and BBB function[39–45], and disrupted Pdgfb–Pdgfr-β signaling induces progressive pericyte loss in ischemic stroke and the aging brain[42,46]. We therefore asked whether a loss of Pdgfb expression could underlie the progressive pericyte loss observed in *Gpr124*-CKO mice. By *in situ* hybridization or RT–qPCR of FACS-sorted brain ECs, we found that *Pdgfb* mRNA was significantly decreased in EC-specific *Gpr124*-CKO mice 1 d after stroke, as compared to that in EC het controls (Fig. 3e,f), consonant with the rapid detachment and progressive loss of pericytes in these mice. Notably, EC-specific constitutive β-catenin activation increased endothelial *Pdgfb* expression by >60% (Fig. 3g). The concomitant loss of perivascular laminin and collagen IV (col IV) in EC *Gpr124*-CKO mice was also rescued by constitutive β-catenin activation (Fig. 3h,i). The expression of *Glut1*, a Gpr124 target gene in embryos[16,17], was not different between *Gpr124*-CKO and het mice, either with or without stroke (Supplementary Figs. 3 and 12a,b). Notably, despite the BBB leak and hemorrhage observed in *Gpr124*-deleted mice after stroke and that angiogenesis occurs within the first week following stroke[47], poststroke microvessel density did not differ between global *Gpr124*-CKO or EC *Gpr124*-CKO mice and their respective control het mice, after correction for edema (Fig. 3j,k and Supplementary Fig. 12c). Thus, the profound effects of *Gpr124* deletion on BBB integrity, hemorrhage, tight junctions, pericyte and ECM occur independently of effects on angiogenesis; this conclusion is consistent with the extremely rapid onset of BBB leak in *Gpr124*-CKO mice at 1 h postreperfusion (Fig. 1i,j and Supplementary Fig. 5d,*e*).

Endothelial Gpr124 deficiency increases tumor hemorrhage and reduces survival during experimental glioblastoma

Next, we examined the effects of *Gpr124* deficiency in glioblastoma (Fig. 4), CNS pathology with impaired microvascular integrity[48] that, unlike tMCAO, does not have an ischemia-reperfusion component. Upon orthotopic intracerebral injection of syngeneic C57Bl/6 GL261 glioblastoma (GBM) cells, Gpr124 was expressed throughout tumor capillaries, similarly to its expression in capillaries of normal brain tissue (Fig. 4a,b). Similarly to Gpr124 expression in mice, GPR124 was expressed in blood vessels in human normal brain and in GBM samples (Supplementary Fig. 13). GL261 tumor-bearing global *Gpr124*-CKO mice (fully backcrossed to C57Bl/6J) showed significantly decreased survival as compared to global het mice (Fig. 4c), with substantially increased intratumoral hemorrhage and edema (Fig. 4d,g). *Gpr124* mRNA expression was strongly decreased (>95%) in ECs isolated from EC *Gpr124*-CKO tumors as compared to EC het tumors; moreover, a modest (20%) decrease in *Gpr124* mRNA expression was observed in tumor as compared to nontumor endothelium in ECs isolated from EC het mice (Fig. 4e). EC-specific *Gpr124*-CKO mice fully recapitulated the hemorrhagic tumor phenotype of global *Gpr124*-CKO mice (Fig. 4f,g). Tumor volumes in global and EC *Gpr124*-CKO mice were not significantly different from those in het control mice, after correction for edema (Fig. 4h,i).

Author Manuscript Author Manuscript Author Manuscript Author Manuscript

Constitutive Wnt–β-catenin-signaling activation rescues *Gpr124*-CKO-associated tumor hemorrhage and vascular phenotypes

We next asked whether, as in ischemic stroke, the *Gpr124*-CKO hemorrhagic phenotype in GBM was associated with decreased endothelial Wnt signaling and could be rescued by constitutive endothelial β-catenin activation. We found that expression of the Wnt targets *Axin2* and *Apcdd1* was decreased in GL261 tumor ECs as compared to normal brain ECs in *Gpr124*-het mice, and their expression was further decreased by EC-specific *Gpr124* deletion (Fig. 5a). Furthermore, endothelial-specific constitutive activation of β-catenin signaling rescued the tumor hemorrhage, BBB breakdown (as assessed by mouse IgG extravasation) and edema phenotypes of EC *Gpr124*-CKO mice (Fig. 5b–d). The increased tumor volume in EC *Gpr124*-CKO mice as compared to EC het mice was likely due to edema, because this difference was negated by correcting for this parameter (Fig. 5e,f). Tumor microvessel density was significantly decreased in EC *Gpr124*-CKO mice after correction for edema (Fig. 5g), which suggests a dual effect of Gpr124 deletion on both BBB integrity and angiogenesis. EC-specific Gpr124 deletion modestly affected tumor vessel morphology, leading to increased vessel diameter (Supplementary Fig. 14). Notably, constitutively active β-catenin expression normalized vessel diameter in EC *Gpr124*-CKO mice (Supplementary Fig. 14), but did not rescue tumor microvessel area density (Fig. 5g).

The cellular and molecular consequences of defective Gpr124– Wnt signaling in the GL261 GBM model were similar to those in the tMCAO model. Tumor vessels in EC *Gpr124*-CKO mice exhibited decreased levels of the tight-junction protein Cldn5, decreased Pdgfr-β^+ and desmin$^+$ pericyte coverage and decreased amounts of the perivascular ECM molecules laminin and collagen IV (col IV), as compared to EC het controls; all of these endpoints were rescued by EC-specific constitutive β-catenin activation (Fig. 6a–d,f,g). *Pdgfb* mRNA expression was decreased by ~40% in tumor ECs from EC *Gpr124*-CKO mice as compared to those from het mice (Fig. 6e). We showed above that *Pdgfb* mRNA expression could be increased by >60% in the ECs of mice with constitutive β-catenin activation under homeostatic conditions (Fig. 3g). These data suggest impaired Pdgfb–Pdgfr-β signaling as a potential mechanism for tumor pericyte loss in EC *Gpr124*-CKO mice. Tumor microvessels in EC *Gpr124*-CKO mice substantially lacked expression of the BBB marker Glut1, similarly to embryonic *Gpr124* deletion[16–18], and this defect was fully rescued by endothelial-specific constitutive β-catenin activation (Fig. 6h,i). By contrast, Glut1 expression in tumor cells, which occurred distally to vessels, was strongly increased in tumors of EC *Gpr124*-CKO mice, and this expression was decreased by concomitant EC β-catenin activation (Fig. 6h; Supplementary Fig. 15a). These results are reminiscent of compensatory neuroepithelial Glut1 upregulation observed in *Gpr124* knockout embryos[16–18] and possibly reflects hypoxic regulation of Glut1 in tumor cells[49,50]. Tumor cell proliferation, as assessed by Ki67 IF staining, was decreased in *Gpr124*-CKO mice (Supplementary Fig. 15b,c). Thus, in a setting of highly angiogenic glioblastoma, endothelial-specific *Gpr124* deletion impairs both BBB integrity and tumor angiogenesis, in contrast to the setting of acute stroke, whereas the effects of endothelial-specific *Gpr124* deletion on BBB function are dissociated from its effects on angiogenesis.

Author Manuscript Author Manuscript Author Manuscript Author Manuscript

DISCUSSION

The mechanisms underlying adult BBB function and cerebrovascular integrity during pathologic conditions are of crucial importance, but are poorly understood. We identified the endothelial receptor Gpr124 as a pleiotropic regulator of adult brain BBB integrity during pathologic injury. Neither the postnatal nor adult cerebrovasculature requires Gpr124 for homeostatic function, but Gpr124 deficiency in pathologic conditions—ischemic stroke and glioblastoma—unmasks a pronounced cell-intrinsic endothelial susceptibility to microvascular damage, with pronounced BBB leak and hemorrhage accompanied by pericyte, ECM and tight-junction deficits.

The similar phenotypes of *Gpr124*$^{-/-}$ and *Wnt7a*$^{-/-}$;*Wnt7b*$^{-/-}$ embryos, both of which show angiogenic arrest and lack of BBB maturation, suggested that Gpr124–Wnt-mediated BBB formation may be obligately coupled to CNS angiogenesis[8,9,16–18]. Indeed, in the highly angiogenic settings of embryogenesis[16–18] or glioblastoma (the current study), endothelial-specific *Gpr124* deletion induces hemorrhage and impairs BBB integrity, Glut1 expression and angiogenesis in parallel. However, in the acute tMCAO stroke model, where angiogenesis occurs at comparatively modest levels within the first week after injury[47], endothelial-specific *Gpr124* deletion does not impair angiogenesis, yet induces profound BBB compromise with edema, hemorrhage and multiple pericyte, ECM and tight-junction deficits. Furthermore, we observed Gpr124-dependent BBB leak within 1 h of reperfusion in the tMCAO model, a time point at which angiogenesis is unlikely to be occurring. Thus, Gpr124 regulation of vascular integrity and angiogenesis are not obligately linked and can, in fact, be dissociated in adult pathologic settings. Endothelial Gpr124 overexpression results in CNS-specific hypervascularity[16], the effects of which in a stroke setting would be of interest to explore.

Our work indicates that a Gpr124–Wnt signaling axis, initially identified during embryonic CNS angiogenesis[20,28,29], also globally maintains BBB functional characteristics during injury in the adult. We found that adult EC-specific *Gpr124* deletion led to decreased expression of numerous neurovascular Wnt target genes, such as *Axin2*, *Apcdd1* and *Cldn5*, in parallel with decreased expression of a multigenic BBB Wnt signature. Crucially, in both the stroke and GBM models, seminal BBB characteristics that are impaired by adult EC-specific *Gpr124* deletion—overall BBB integrity, pericyte coverage, ECM deposition, tight-junction protein production and Wnt targetgene expression—are each strongly rescued by EC-specific constitutive activation of Wnt signaling via activated β-catenin (Fig. 6j). In the GBM setting, expression of activated β-catenin rescued the effects of *Gpr124* deletion on tumor vessel diameter but not microvessel density, which suggests that there is additional complexity to the mechanisms by which Gpr124 regulates angiogenesis in this setting. Our data represent the first demonstration, to our knowledge, that acute endothelial β-catenin activation in adult mice is sufficient to protect against BBB breakdown and improve neurological outcomes after ischemic stroke, a finding that might have translational implications.

It is not known whether Gpr124 regulation of Wnt7a and Wnt7b signaling during embryogenesis and in cultured cells[20,28,29] occurs by direct or indirect mechanisms. The

Author Manuscript Author Manuscript Author Manuscript Author Manuscript

glycosylphosphatidylinisotol (GPI)-anchored protein Reck has been reported to modulate Gpr124–Wnt7 signaling, again through unclear mechanisms[20,51]. Intriguingly, global *Reck*$^{+/-}$ mice display augmented brain-tissue damage after ischemic stroke, although the endothelial-cell-autonomous role of Reck remains unclear[52]. The Gpr124 independence of the adult cerebrovasculature in homeostasis strongly contrasts with its Gpr124 dependence during injury. In this respect, Wnt signaling components such as Norrin and Fzd4 exhibit functional redundancy with Gpr124 during embryonic and postnatal BBB development[8,9,12,14]. Given that Norrin and Fzd4 are abundantly expressed in adult brain vasculature[53–55], these proteins could conceivably exhibit redundancy with Gpr124 during homeostasis but not disease states in the adult. Our data are consistent with a model in which disease states reduce endothelial Wnt signaling to a level insufficient to maintain a functional BBB, which results in low-grade BBB leak without hemorrhage. *Gpr124* deletion during pathology further reduces endothelial Wnt signaling, which results in high-grade BBB dysfunction and hemorrhage (Supplementary Fig. 16).

Multiple pericyte, ECM and tight-junction outputs might, in coordination, underlie the BBB dysfunction arising from *Gpr124* deficiency (Fig. 6j). The Gpr124-regulated and activated β-catenin-reversible BBB defects in tight-junction protein expression, pericyte coverage and ECM synthesis have each been reported to be individually sufficient in loss-of-function settings to induce BBB leak and/or CNS hemorrhage. Given that claudin-5 deficiency impairs BBB integrity, and that laminin γ1 or collagen IV deficiency leads to spontaneous intracerebral hemorrhage[56–58], dysregulation of these proteins in endothelial-specific *Gpr124*-deleted mice could facilitate pathologic BBB compromise. Similarly, endothelial *Gpr124* deletion is associated with reduced EC *Pdgfb* mRNA, which could underlie the marked and progressive pericyte loss during stroke or tumor, in an analogy to the decreased pericyte coverage and BBB integrity observed upon impaired Pdgfb–Pdgfr-β signaling during ischemic stroke[46] and glioblastoma[27]. ECM loss during stroke and glioblastoma in endothelial-specific *Gpr124*-deleted mice could be secondary to loss of pericytes, which regulate perivascular ECM production[59]. The observation that Gpr124 deletion leads to loss of the BBB marker Glut1 during embryogenesis[16,17,28], and in glioblastoma, but not in stroke, represents an interesting dichotomy, because the former two settings are strongly neoangiogenic. *Glut1* deficiency causes BBB breakdown in neonates[60] and could thus underlie the effects of Gpr124 deficiency on the BBB during both embryogenesis and tumorigenesis.

Overall, our findings indicate that the Gpr124–Wnt signaling axis functions as an essential defense mechanism deployed by the adult cerebrovasculature to protect BBB function and vascular integrity under pathologic stress conditions. Given the substantial deleterious consequences of BBB dysfunction during CNS disorders such as stroke, cancer and multiple sclerosis[1–3], the Gpr124–Wnt pathway represents a novel opportunity for the therapeutic manipulation of cerebrovascular integrity.

Author Manuscript Author Manuscript Author Manuscript Author Manuscript

ONLINE METHODS

Generation of the Gpr124 conditional-knockout allele

For targeting exon 1 of the *Gpr124* locus, a 10.1-kb SnaBI region of mouse genomic DNA (from the 129 strain) containing the first coding exon of *Gpr124* was cloned into the plasmid pKS (Stratagene) with diphtheria toxin A (DTA) used as a negative-selection marker. The first coding exon was "floxed" (flanked with *LoxP* sites) by cloning a single *LoxP* site 5′ to the target sequence and a *LoxP* site with a neomycin selection cassette 3′ to the target sequence. Targeting constructs were electroporated into 129 mouse embryonic stem cells for targeting of the endogenous locus by homologous recombination (Supplementary Fig. 1a). The DTA cassette, located outside of the homology arm, served as a negative-selection marker against random insertion, whereas the neomycin cassette within the homology arms served as a positive-selection marker when the electroporated ES cells were grown in ES media containing 250 μg/ml G418. Correctly targeted clones were identified by PCR; one primer was located within the positive-selection cassette or recombinant sequence flanking the single *LoxP* site, and the other primer was located outside of the homology arms on both sides of the cassettes. An added benefit of this PCR strategy was that it ensured that the single *LoxP* was included in the homologous recombination event. Correctly targeted clones were confirmed on the 5′ and 3′ sides by Southern blot, using probes located outside of the homology arms (Supplementary Fig. 1b). Correctly targeted clones were injected into C57Bl/6 mouse blastocysts. Chimeras with >90% agouti coat color were crossed to C57Bl/6 females, and germ-line transmission was confirmed in agouti F1 pups by tail-tip PCR. The *Gpr124* exon 1 floxed allele was backcrossed into the C57Bl/6 background for more than six generations with the assistance of MAX BAX accelerated backcrossing services (http://www.jax.com); the allele has been maintained in C57Bl/6 for more than 4 years.

Animals and treatment

Animals were housed in a pathogen-free animal facility with 12-h light and dark cycles. All animal studies were performed in accordance with the National Institutes of Health guidelines for use, and care of live animals and were approved by the Institutional Animal Care and Use Committee at Stanford University. The $Gpr124^{flox}$ allele and the constitutively deleted $Gpr124^{lacZ}$ allele[16] (referred to as $Gpr124^{-}$) were crossed with the global tamoxifen-inducible driver *ROSA-CreER* allele[61] or the endothelial tamoxifen-inducible driver Cdh5-CreER (Ralf Adams)[32], all fully in the C57Bl/6 background, to generate $Gpr124^{flox/-}$;*ROSA-CreER* mice (global *Gpr124* CKO) and $Gpr124^{flox/+}$;*ROSA-CreER* mice (global *Gpr124* het) or $Gpr124^{flox/-}$; *Cdh5-CreER* mice (EC *Gpr124* CKO) and $Gpr124^{flox/+}$; *Cdh5-CreER* mice (EC *Gpr124* het), respectively. To induce endothelial β-catenin constitutive activation in conjunction with Gpr124 cko, $Gpr124^{+/-}$;*Cdh5-CreER* mice were crossed with mice bearing the $Ctnnb1^{lox(ex3)}$ allele[37] to generate $Gpr124^{+/-}$;$Ctnnb1^{lox(ex3)/+}$; *Cdh5-CreER* mice, which were then crossed with $Gpr124^{flox/flox}$ mice to generate $Gpr124^{flo/x-}$;$Ctnnb1^{lox(ex3)/+}$; *Cdh5-CreER* (termed CKO; β-cat), $Gpr124^{flox/+}$; $Ctnnb1^{lox(ex3)/+}$;*Cdh5-CreER* (het; β-cat), $Gpr124^{flox/-}$;$Ctnnb1^{+/+}$; *Cdh5-CreER* (CKO) and $Gpr124^{flox/+}$;$Ctnnb1^{+/+}$;*Cdh5-CreER* (het) mice. *Rosa-LSL-TdTomato* mice (stock no. 007905) and BAT-Gal mice[62] (stock no. 005317) were purchased from Jackson Laboratory.

Author Manuscript Author Manuscript Author Manuscript Author Manuscript

For induction of *Gpr124* deletion or β-catenin constitutive activation, 7–8-week-old male and female mice were treated with four doses of tamoxifen (2 mg/10 g body weight) in corn oil through an oral feeding needle every other day for 7 d. Mice were allowed to recover from tamoxifen treatment (undergo washout) for 4 weeks before undergoing any other surgical procedures or experiments.

Sample and subject selection and general experimental practices

Sample sizes for all experiments were predetermined on the basis of extensive laboratory experience with these end points. Animals that survived through the endpoint of the experiments successfully were included in the analysis. This criterion was pre-established (see each animal model section). For all molecular and behavioral experiments, animals were subjected to the same treatment or surgery and grouped on the basis of their genotypes after data collection. Additionally, the investigators were blinded to the genotypes of the mice until all data had been collected.

Mouse GL261 tumor cell implantation and human glioblastoma tissue

Mouse GL261 glioblastoma cells (derived from a C57Bl/6 genetic background) were from the National Cancer Institute Tumor Repository and grown in DMEM supplemented with 10% FCS and Pen-Strep Glutamine in humidified chambers at 37 °C with 5% CO_2. Cells were trypsinized and resuspended at 20,000 cells per μl of Leibovitz L-15 media. Cells were implanted into the striatum, 1.8 mm to the right of the bregma, at a depth of 2.8 mm using a stereotactic injection frame over the course of 2 min. The needle was slowly withdrawn at a pace of 0.5 mm every 30 s and the burr hole was sealed with bone wax before closure of skin with a 4-0 silk suture. Both male and female mice were equally used in each group. Mice were followed until moribund, at which point animals were deeply anesthetized with isoflurane and transcardially perfused with heparinized saline (10 U/ml) for 2 min. Tumors were removed, post-fixed in 4% PFA in PBS for 1 h at 4 °C, soaked in 30% sucrose in PBS overnight at 4 °C and then embedded in OCT. Animals were excluded if no tumors were present. This exclusion plan was pre-established. The surgeons performing implantation were blinded to the genotypes of the mice. This cell line was authenticated by the NCI Tumor Repository for negativity for mycoplasma and a genetic-typing test (IDEXX BioResearch's CellCheck) compared the genetic profile of the cells used to that established for this cell line (http://www.idexxbioresearch.com/radil/Technical_Library/Cell_Line_Authentication_/index.html). Deidenitified human glioblastoma specimens were obtained from the Department of Neurosurgery of Stanford School of Medicine under an exemption from the Institutional Review Board (IRB) of Stanford University.

Transient middle cerebral artery occlusion (tMCAO)

Adult mice (males and females equally used in each group, 12–20 weeks old) underwent transient middle cerebral artery occlusion by the intraluminal suture method for 60 min (body temperature maintained at 37 ± 0.5 °C), as previously described[30]. Animals had free access to food and water throughout the reperfusion period. Neurological score was evaluated at 24-h post-MCAO by a blinded observer: 0, normal motor function; 1, flexion of torso and the contralateral forelimb upon lifting by the tail; 2, circling to the ipsilateral side but normal posture at rest; 3, leaning to the ipsilateral side at rest; 4, unable to walk

Author Manuscript Author Manuscript Author Manuscript Author Manuscript

spontaneously. After neurological testing, the mice were deeply anesthetized with isoflurane and were transcardially perfused with ice cold heparinized saline (10 U/ml) for 2 min. The brains were sectioned into 2-mm-thick sections and placed in 2% 2,3,5-triphenyltetrazolium chloride (TTC, cat. #T8877, Sigma-Aldrich, St. Louis, MO) for 10 min at 37 °C to delineate infarcts. Infarct areas were determined using an image analysis system (ImageJ) and corrected for edema. The presence of hemorrhage was recorded at the time of premature death, morbidity or sacrifice at day 7. The tissue was placed in 4% PFA for 1 h at room temperature and then transferred to 70% ethanol for paraffin embedding or to 30% sucrose in PBS overnight at 4 °C before embedding in OCT. Animals were excluded if no neurological deficits were present after surgery. This exclusion plan was pre-established. The persons performing the surgery and recording neurological scores were blinded to the genotypes of the mice.

Immunofluorescence analysis

Frozen sections 10 μm or 12 μm in thickness were allowed to dry on Superfrost Plus slides (Fisher) at room temperature before being rehydrated in 1X PBS. Tissue were blocked in 5% Normal Goat Serum (Jackson ImmunoResearch, West Grove, PA) in PBS + 1% BSA + 0.3% Triton X-100 for 30 min at room temperature. Samples were incubated at 4 °C with the following primary antibodies in PBS + 1% BSA + 0.3% Triton X-100 + 0.1% NaN_3: hamster anti-mouse CD31 (1:100, cat. #MAB1398Z, Millipore, Billerica, MA), rat anti-mouse Pdgfrβ (1:50, cat. # 14-1402-82, Clone APB5, eBiosciences, San Diego, CA), rabbit anti-claudin-5 (1:100, cat. # 34-1600, Thermo Fisher Scientific, MA), rabbit anti-Glut-1 (1:50, cat. #400060, Millipore, Billerica, MA), rabbit anti-β-galactosidase (1:1,000, cat. #559761, MP Biomedicals, Solon, OH), rabbit anti-fibrinogen (1:200, cat. # ab34269, Abcam, Cambridge, MA), rabbit anti-Desmin (1:200, cat. #ab15200, Abcam, Cambridge, MA), rabbit anti-laminin (1:200, cat. # L9393, Sigma-Aldrich, St. Louis, MO), rabbit anticollagen type IV (1:100, cat. # ab6586, Abcam, Cambridge, MA), rabbit anti-Ki67 monoclonal antibody (1:200, clone SP6, Thermo Fisher Scientific, MA). Polyclonal rabbit anti-Gpr124 (1:100) was generated previously[16]. AlexaFluor 488 Isolectin GS-IB4 (1:200, cat. # 121411, Life Technologies, Grand Island, NY) was used similarly to mark endothelial cells when applicable.

Excess antibody was removed by rinsing in PBS + 0.1% Triton X-100 for 10 min, 4 times. Samples were then incubated at room temperature for 1 h with the following secondary fluorescently labeled antibodies: FITC or Cy3 goat antihamster IgG, FITC or Cy3 goat anti-rat IgG, FITC or Cy3 goat anti-rabbit IgG, Cy3 goat anti-mouse IgG, FITC or Cy3 streptavidin (Jackson ImmunoResearch, West Grove, PA) diluted 1:400 in PBS + 1% BSA + 0.3% Triton X-100 for 1 h at room temperature. Excess antibody was removed by rinsing in PBS + 0.1% Triton X-100 for 10 min, four times. Slides were mounted in Vectashield mounting medium with DAPI (Vector labs, Burlingame, CA) and imaged with a Zeiss Z1 Axioimager with ApoTome attachment to obtain 10×, 20× or 40× images. Immunofluorescence signal area or density was quantified by ImageJ and normalized by vessel area (CD31 signal area). Pericyte coverage was quantified by measuring the IF staining signal length of pericyte or endothelial profile with the NeuronJ plugin for ImageJ.

Author Manuscript Author Manuscript Author Manuscript Author Manuscript

Determination of BBB integrity

For sulfo-NHS-biotin perfusion, mice were deeply anesthetized with isoflurane. The beating heart was perfused via the left ventricle with 50 ml EZ-link-sulfo-NHS-biotin (0.5 mg/ml, cat. # 21217, Thermo Scientific, MA) in 1× PBS with Ca^{2+} and Mg^{2+} (GIBCO) over the course of 5 min, followed with perfusion of 50 ml ice-cold 1% PFA in PBS. Brains were then fixed in 4% PFA for 1 h at room temperature and cut into 2-mm-thick slices and transferred to 30% sucrose in PBS overnight at 4 °C before embedding in OCT. Frozen sections 10 μm in thickness were stained as described above with Cy3-strepavidin and FITC-CD31 or isolectin.

For Evans blue perfusion, 100 μl 2% Evans blue (cat. # E-2129, Sigma-Aldrich, MO) was injected i.v. retroorbitally. After 24 h, the mice were deeply anesthetized with isoflurane followed by transcardial perfusion into the beating heart via the left ventricle with 50 ml ice-cold PBS to remove the intravascular dye. The brains were divided into ipsilateral ischemic hemispheres and contralateral nonischemic hemispheres and then were homogenized in 1 ml of 50% trichloroacetic acid and centrifuged (10,000 rpm, 20 min). The supernatant was diluted fourfold with ethanol. The concentrations of Evans blue were measured with a fluorescence reader (620 nm excitation; 680 nm emission) and presented as ng per mg brain tissue.

Extravasation of plasma mouse IgG or fibrinogen was determined with immunofluorescence staining, as described above.

Histological analysis

Brain tissues were fixed in 4% PFA in PBS at room temperature for 1 h and transferred into 70% ethanol and embedded in paraffin. 5-μm-thick sections were obtained using a paraffin microtome with stainless-steel knives. The sections were mounted on glass slides, deparaffinized with xylene, dehydrated through graded series of ethanol and stained with hematoxylin–eosin.

Perl's iron staining

Perl's iron staining was performed on 5-μm-thick paraffin-embedded specimens, as previously described[30]. Briefly, diaminobenzidine-enhanced Perl's iron staining was conducted in deparaffinized tissue by incubation in 1% KFeCN/1% HCl for 15 min followed by methyl green counterstain.

Electron microscopy

Specimens from mice were fixed in 2.5% glutaraldehyde in 0.1 M cacodylate buffer (pH 7.4), dehydrated, embedded in epoxy resin and visualized with a JEOL (model JEM1400) transmission-electron microscope with a LaB6 emitter at 120 kV, and processed at the Stanford Electron Microscopy facility.

FACS sorting and analysis of brain ECs

Brains of 12–24 week-old adult mice (male and female mice were both used) were minced with a razor blade and disaggregated in Type IV collagenase (400 U/ml, Worthington,

Author Manuscript Author Manuscript Author Manuscript Author Manuscript

Lakewood, NJ), Dispase (1.2 U/ml, Worthington, Lakewood, NJ) and DNase I (32 U/ml, Worthington, Lakewood, NJ) in 6 mL 1× PBS with Ca^{2+} and Mg^{2+} (GIBCO) at 37 °C for 60 min, with gentle trituration every 10 min. After adequate disaggregation, 1 ml of FBS (FBS) was added to the disaggregation reaction and the disaggregated cells were washed with 1× ice-cold PBS and filtered through a 40-μm mesh. After centrifugation at 400*g* for 5 min, cell pellets were resuspended in 10 ml 20% BSA and centrifuged at 1,000*g* at 4 °C for 25 min to remove the myelin. The pellets were then resuspended in 1× PBS/3% FBS/0.1% NaN_3/2 mM EDTA and blocked with rat anti-mouse CD16/32 (Mouse BD Fc Block, BD Pharmingen) for 5 min on ice. Endothelial cells were labeled with PE-Cyanine7 rat anti-mouse CD31 (cat. # 25-0311-82, eBiosciences, CA), and pericytes were labeled with APC rat anti-mouse Pdgfrβ (cat. # 17-1402-82, eBiosciences, CA). PE rat anti-mouse CD45 (cat. #516087, BD Pharmingen, CA) and 7-AAD (Invitrogen) were added to exclude hematopoietic lineage cells and dead cells. Staining was done for 1 h at 4 °C. Cells were washed and PE-cyanine7-$CD31^+$/APC-$Pdgfr\beta^-$/PE-$CD45^-$/7-AAD^- cells were sorted into EGM-2/MV medium (cat. # CC3202, Clontech, Mountain View, CA) with an Aria II sorter (BD) or analyzed with an LSRII analyzer (BD) at the Stanford University Shared FACS Facility, and FACS data were analyzed using FlowJo software (TreeStar). Cells were centrifuged at 2,000g at 4 °C for 10 min and resuspended in Trizol (Life Technologies) or extraction buffer of the Arcturus PicoPure RNA Isolation Kit (Applied Biosystems) for RNA extraction.

Primary brain EC culture and adenovirus infection

Brains of 12–24-weekold adult mice were minced and disaggregated as described above. After centrifugation at 400*g* for 5 min, cell pellets were resuspended in EGM-2 MV medium (cat. # CC3202, Clontech, Mountain View, CA) with 10% FBS and 4 μg/ml puromycin (to kill all the other cell types except brain ECs) and plated into fibronectin-precoated plates (10 μg/ml for 30 min at 37 °C). 2–3 d later, medium was discarded and cells were washed with PBS twice and medium was replaced with EGM-2 MV/10% FBS. The purity of isolated brain ECs was confirmed by CD31 and VE-cadherin immunofluorescence staining (>90% purity), with minimal contamination of pericytes (Pdgfr-β positive).

After 5 d in culture, primary brain ECs were infected with adenovirus expressing mouse IgG2α Fc fragment (Ad Fc) or mouse Wnt7b (Ad Wnt7b) at an multiplicity of infection (MOI) 50:1 for 2 d before being lysed in Trizol for RNA extraction. Ad Fc has been described previously[63]. Mouse Wnt7b cDNA was cloned in Add2 shuttle vector first and then cloned into the E1 region of $E1^-E3^-$ Ad strain 5 by homologous recombination, followed by Ad production in 293 cells and CsCl gradient purification of virus, as described[63].

Pdgfb mRNA *in situ* hybridization

Pdgfb mRNA transcripts were detected using the RNAscope 2.5 HD Reagent Kit RED (cat. # 322360, Advanced Cell Diagnostics, CA) and corresponding probe (cat. # 424651, Advanced Cell Diagnostics, CA) on 4% PFA fixed frozen tissue sections per the manufacturer's instructions. A negative-control probe (DapB, cat. # 310043, Advanced Cell Diagnostics, CA) was included in the assay.

Author Manuscript Author Manuscript Author Manuscript Author Manuscript

Real-time quantitative PCR (RT–qPCR)

Total RNA was extracted using the Direct-zol RNA MiniPrep kit (Zymo Research, Irvine, CA). RNA was reverse transcribed using iScript Reverse Transcription Supermix for RT–qPCR according to the manufacturer's instructions (BIO-RAD, Hercules, CA). RT–qPCR was carried out on a StepOnePlus Real-Time PCR System using the Power SYBR Green method (Applied Biosystems). RNA expression was calculated using the comparative *Ct* method normalized to β-actin. Data were expressed relative to a calibrator using the $2^{-(\Delta\Delta Ct)} \pm s$ formula. Primer sequences for β-actin, *Axin2* and *Cldn5* are from a previous study[21]. The primer sequences for other genes are available from the Harvard PrimerBank upon request.

RNA-seq

RNA extraction and 3′-seq—For brain ECs of global *Gpr124*-CKO versus het mice, total RNA was extracted using the Arcturus PicoPure RNA Isolation Kit (Applied Biosystems). 3′-end sequencing for expression quantification (3′-end seq) was performed as described[64]. In brief, mRNA was first enriched from total RNA by poly-A selection to remove ribosomal RNA and other non-poly-A RNA. The mRNA was then fragmented to 100–200 bases. Oligo-dT-directed reverse transcription generated complementary DNAs corresponding to the 3′end of poly-A transcripts; the complementary DNA was amplified by PCR using the Ovation 3′-DGE System kit (NuGen Technologies, San Carlos, CA). Amplified cDNA was sheared using a Covaris ultrasonicator and then libraries were prepared using the Ovation SP + Ultralow DR Multiplex System (NuGen Technologies, San Carlos, CA). Deep sequencing was then performed on the Illumina Hiseq-2500 platform (Illumina, Hayward, CA) in single-end 50 bp format.

For brain ECs of β-cat versus WT mice, RNA was extracted using the Qiagen RNeasy Kit followed by DNaseI (Qiagen, Valencia, CA) treatment. cDNA libraries were generated using the NuGEN Ovation RNA-Seq System V2 (NuGen Technologies, San Carlos, CA). The amplified product (ds DNA) was fragmented to ~200–300 bp using the E220 Focused Ultrasonicator (Covaris, Woburn, MA). Indexed libraries were generated following end repair, adaptor ligation and PCR amplification using the NEBNext Ultra RNA library prep kit for Illumina (New England Biolabs, Ipswich, MA). The indexed cDNA libraries were sequenced (paired end, 100 bp) on an Illumina HiSeq2000 platform.

RNA-seq data analysis—Raw sequence reads were mapped to the mouse genome (mm10) using TopHat, and the frequency of Refseq genes was counted using customized R scripts. The raw counts were then normalized using the trimmed mean of M values (TMM) method and compared using the Bioconductor package "edgeR". Reads per kilobase per million (RPKM) mapped reads were also calculated from the raw counts. Differentially expressed genes were identified if RPKM ≥ 1 in at least one sample, fold change was ≥ 1.5, and $P \leq 0.05$. Gene enrichments were analyzed using DAVID (database for annotation, visualization, and integrated discovery; http://david.abcc.ncifcrf.gov), which is a bioinformatic resource for functional interpretation of large lists of genes. Hierarchical-clustering analysis was performed in Cluster 3.0 using the average-linkage clustering method. The results were then visualized in Treeview, and a heat map was generated.

Author Manuscript Author Manuscript Author Manuscript Author Manuscript

Differentially expressed (DE) gene lists from the group comparison mentioned above were uploaded to DAVID v6.7 to identify enriched biological themes, such as GO terms and KEGG pathways.

Statistical analysis

Assumptions concerning the data (for example, normal distribution and similar variation between experimental groups) were examined for appropriateness before statistical tests were conducted. Statistical analysis was performed using the GraphPad Prism software package. All statistical tests use biological replicates and are indicated by group size (n) in figure legends. Results were expressed as mean ± s.e.m. (standard error of mean). Significance ($P < 0.05$) between two groups was calculated using an unpaired Student's t-test (two-tailed) or paired Student's t-test for two groups of values representing paired observations. Significance between two Kaplan–Meier survival curves was calculated using log–rank test.

Data availability

Data are available from the corresponding authors upon request. The Gene Expression Omnibus (GEO) accession code for the data in this manuscript is GSE74052.

Supplementary Material

Refer to Web version on PubMed Central for supplementary material.

Acknowledgments

We are grateful to members of the Kuo laboratory, J. Yang and P. Han for helpful comments. We thank P. Chu (Stanford Histology Core Facility), J. Perrino (Stanford Electron Microscopy Facility) and C. Crumpton, T. Knaak, B. Gomez, O. Herman and M. Bigos (Stanford Shared FACS Facility). FACS sorting and analysis used instruments in the Shared FACS Facility, obtained using NIH S10 Shared Instrument Grant (S10RR025518-01, S10RR027431-01) to the Stanford Shared FACS Facility. We thank M. Edwards (Department of Neurosurgery, Stanford University) for providing the human glioblastoma specimens. We thank R. Adams (Max Planck Institute for Molecular Biomedicine) for providing the Cdh5-CreER mice. We thank the National Cancer Institute–DCTD Repository for providing the GL261 cell line. J.C. was supported by an American Heart Association Postdoctoral Fellowship (15POST23020039) and M.R.M. was supported by the Stanford Medical Scientist Training Program (NIGMS GM07365). J.H.Z. was supported by a Howard Hughes Medical Institute Medical Research Fellows Program grant. H.Y.C. was supported by NIH grant P50-HG007735. This work was also supported by American Heart Association Innovative Science Award 12PILT12850014, a Stanford Stroke Collaborative Action Network Pilot Grant and NIH grants R01HL074267, R01NS064517, U01DK085527 and R01CA158528 to C.J.K.

References

1. Obermeier B, Daneman R, Ransohoff RM. Development, maintenance and disruption of the blood-brain barrier. Nat Med. 2013; 19:1584–1596. [PubMed: 24309662]
2. Engelhardt B, Liebner S. Novel insights into the development and maintenance of the blood-brain barrier. Cell Tissue Res. 2014; 355:687–699. [PubMed: 24590145]
3. Dejana E, Nyqvist D. News from the brain: the GPR124 orphan receptor directs brain-specific angiogenesis. Sci Transl Med. 2010; 2:58ps53.
4. McCarty JH, et al. Selective ablation of alphav integrins in the central nervous system leads to cerebral hemorrhage, seizures, axonal degeneration and premature death. Development. 2005; 132:165–176. [PubMed: 15576410]

Author Manuscript Author Manuscript Author Manuscript Author Manuscript

5. Proctor JM, Zang K, Wang D, Wang R, Reichardt LF. Vascular development of the brain requires beta8 integrin expression in the neuroepithelium. J Neurosci. 2005; 25:9940–9948. [PubMed: 16251442]
6. Ben-Zvi A, et al. Mfsd2a is critical for the formation and function of the blood-brain barrier. Nature. 2014; 509:507–511. [PubMed: 24828040]
7. Vallon M, Chang J, Zhang H, Kuo CJ. Developmental and pathological angiogenesis in the central nervous system. Cell Mol Life Sci. 2014; 71:3489–3506. [PubMed: 24760128]
8. Stenman JM, et al. Canonical Wnt signaling regulates organ-specific assembly and differentiation of CNS vasculature. Science. 2008; 322:1247–1250. [PubMed: 19023080]
9. Daneman R, et al. Wnt/beta-catenin signaling is required for CNS, but not non- CNS, angiogenesis. Proc Natl Acad Sci USA. 2009; 106:641–646. [PubMed: 19129494]
10. Xu Q, et al. Vascular development in the retina and inner ear: control by Norrin and Frizzled-4, a high-affinity ligand-receptor pair. Cell. 2004; 116:883–895. [PubMed: 15035989]
11. Ye X, et al. Norrin, frizzled-4, and Lrp5 signaling in endothelial cells controls a genetic program for retinal vascularization. Cell. 2009; 139:285–298. [PubMed: 19837032]
12. Wang Y, et al. Norrin/Frizzled4 signaling in retinal vascular development and blood brain barrier plasticity. Cell. 2012; 151:1332–1344. [PubMed: 23217714]
13. Paes KT, et al. Frizzled 4 is required for retinal angiogenesis and maintenance of the blood-retina barrier. Invest Ophthalmol Vis Sci. 2011; 52:6452–6461. [PubMed: 21743011]
14. Zhou Y, et al. Canonical WNT signaling components in vascular development and barrier formation. J Clin Invest. 2014; 124:3825–3846. [PubMed: 25083995]
15. Junge HJ, et al. TSPAN12 regulates retinal vascular development by promoting Norrin- but not Wnt-induced FZD4/β-catenin signaling. Cell. 2009; 139:299–311. [PubMed: 19837033]
16. Kuhnert F, et al. Essential regulation of CNS angiogenesis by the orphan G protein-coupled receptor GPR124. Science. 2010; 330:985–989. [PubMed: 21071672]
17. Cullen M, et al. GPR124, an orphan G protein-coupled receptor, is required for CNS-specific vascularization and establishment of the blood-brain barrier. Proc Natl Acad Sci USA. 2011; 108:5759–5764. [PubMed: 21421844]
18. Anderson KD, et al. Angiogenic sprouting into neural tissue requires Gpr124, an orphan G protein-coupled receptor. Proc Natl Acad Sci USA. 2011; 108:2807–2812. [PubMed: 21282641]
19. Chandana EP, et al. Involvement of the Reck tumor suppressor protein in maternal and embryonic vascular remodeling in mice. BMC Dev Biol. 2010; 10:84. [PubMed: 20691046]
20. Vanhollebeke B, et al. Tip cell-specific requirement for an atypical Gpr124- and Reck-dependent Wnt/β-catenin pathway during brain angiogenesis. eLife. 2015; 4:e06489.
21. Liebner S, et al. Wnt/β-catenin signaling controls development of the blood-brain barrier. J Cell Biol. 2008; 183:409–417. [PubMed: 18955553]
22. Lippmann ES, et al. Derivation of blood-brain barrier endothelial cells from human pluripotent stem cells. Nat Biotechnol. 2012; 30:783–791. [PubMed: 22729031]
23. Paolinelli R, et al. Wnt activation of immortalized brain endothelial cells as a tool for generating a standardized model of the blood brain barrier in vitro. PLoS One. 2013; 8:e70233. [PubMed: 23940549]
24. Tran KA, et al. Endothelial β-catenin signaling is required for maintaining adult blood-brain barrier integrity and central nervous system homeostasis. Circulation. 2016; 133:177–186. [PubMed: 26538583]
25. Wang W, et al. GSK-3β inhibitor TWS119 attenuates rtPA-induced hemorrhagic transformation and activates the Wnt/β-catenin signaling pathway after acute ischemic stroke in rats. Mol Neurobiol. 2016; 53:7028–7036. [PubMed: 26671619]
26. Wu C, et al. Wnt/β-catenin coupled with HIF-1α/VEGF signaling pathways involved in galangin neurovascular unit protection from focal cerebral ischemia. Sci Rep. 2015; 5:16151. [PubMed: 26537366]
27. Reis M, et al. Endothelial Wnt/β-catenin signaling inhibits glioma angiogenesis and normalizes tumor blood vessels by inducing PDGF-B expression. J Exp Med. 2012; 209:1611–1627. [PubMed: 22908324]

Author Manuscript Author Manuscript Author Manuscript Author Manuscript

28. Zhou Y, Nathans J. Gpr124 controls CNS angiogenesis and blood-brain barrier integrity by promoting ligand-specific canonical wnt signaling. Dev Cell. 2014; 31:248–256. [PubMed: 25373781]
29. Posokhova E, et al. GPR124 functions as a WNT7-specific coactivator of canonical β-catenin signaling. Cell Reports. 2015; 10:123–130. [PubMed: 25558062]
30. Maier CM, Hsieh L, Crandall T, Narasimhan P, Chan PH. Evaluating therapeutic targets for reperfusion-related brain hemorrhage. Ann Neurol. 2006; 59:929–938. [PubMed: 16673393]
31. McCullough L, et al. Neuroprotective function of the PGE2 EP2 receptor in cerebral ischemia. J Neurosci. 2004; 24:257–268. [PubMed: 14715958]
32. Wang Y, et al. Ephrin-B2 controls VEGF-induced angiogenesis and lymphangiogenesis. Nature. 2010; 465:483–486. [PubMed: 20445537]
33. Xiong X, et al. IL-4 is required for sex differences in vulnerability to focal ischemia in mice. Stroke. 2015; 46:2271–2276. [PubMed: 26130091]
34. Ritzel RM, Capozzi LA, McCullough LD. Sex, stroke, and inflammation: the potential for estrogen-mediated immunoprotection in stroke. Horm Behav. 2013; 63:238–253. [PubMed: 22561337]
35. Daneman R, et al. The mouse blood-brain barrier transcriptome: a new resource for understanding the development and function of brain endothelial cells. PLoS One. 2010; 5:e13741. [PubMed: 21060791]
36. Moro E, et al. In vivo Wnt signaling tracing through a transgenic biosensor fish reveals novel activity domains. Dev Biol. 2012; 366:327–340. [PubMed: 22546689]
37. Harada N, et al. Intestinal polyposis in mice with a dominant stable mutation of the beta-catenin gene. EMBO J. 1999; 18:5931–5942. [PubMed: 10545105]
38. Huang W, Sherman BT, Lempicki RA. Systematic and integrative analysis of large gene lists using DAVID bioinformatics resources. Nat Protoc. 2009; 4:44–57. [PubMed: 19131956]
39. Lindahl P, Johansson BR, Levéen P, Betsholtz C. Pericyte loss and microaneurysm formation in PDGF-B-deficient mice. Science. 1997; 277:242–245. [PubMed: 9211853]
40. Lindblom P, et al. Endothelial PDGF-B retention is required for proper investment of pericytes in the microvessel wall. Genes Dev. 2003; 17:1835–1840. [PubMed: 12897053]
41. Armulik A, et al. Pericytes regulate the blood-brain barrier. Nature. 2010; 468:557–561. [PubMed: 20944627]
42. Bell RD, et al. Pericytes control key neurovascular functions and neuronal phenotype in the adult brain and during brain aging. Neuron. 2010; 68:409–427. [PubMed: 21040844]
43. Daneman R, Zhou L, Kebede AA, Barres BA. Pericytes are required for blood-brain barrier integrity during embryogenesis. Nature. 2010; 468:562–566. [PubMed: 20944625]
44. Armulik A, Genové G, Betsholtz C. Pericytes: developmental, physiological, and pathological perspectives, problems, and promises. Dev Cell. 2011; 21:193–215. [PubMed: 21839917]
45. Hall CN, et al. Capillary pericytes regulate cerebral blood flow in health and disease. Nature. 2014; 508:55–60. [PubMed: 24670647]
46. Shen J, et al. PDGFR-β as a positive regulator of tissue repair in a mouse model of focal cerebral ischemia. J Cereb Blood Flow Metab. 2012; 32:353–367. [PubMed: 21952111]
47. Hayashi T, Noshita N, Sugawara T, Chan PH. Temporal profile of angiogenesis and expression of related genes in the brain after ischemia. J Cereb Blood Flow Metab. 2003; 23:166–180. [PubMed: 12571448]
48. Carmeliet P, Jain RK. Principles and mechanisms of vessel normalization for cancer and other angiogenic diseases. Nat Rev Drug Discov. 2011; 10:417–427. [PubMed: 21629292]
49. Bürgi, S., et al. *In vivo* imaging of hypoxia-inducible factor regulation in a subcutaneous and orthotopic GL261 glioma tumor model using a reporter gene assay. Mol Imaging. 2014. http://dx.doi.org/10.2310/7290.2014.00029
50. Airley R, et al. Glucose transporter glut-1 expression correlates with tumor hypoxia and predicts metastasis-free survival in advanced carcinoma of the cervix. Clin Cancer Res. 2001; 7:928–934. [PubMed: 11309343]

Author Manuscript Author Manuscript Author Manuscript Author Manuscript

51. Ulrich F, et al. Reck enables cerebrovascular development by promoting canonical Wnt signaling. Development. 2016; 143:1055. [PubMed: 26980794]
52. Wang H, et al. The Reck tumor suppressor protein alleviates tissue damage and promotes functional recovery after transient cerebral ischemia in mice. J Neurochem. 2010; 115:385–398. [PubMed: 20796170]
53. Luhmann UF, et al. Vascular changes in the cerebellum of Norrin/Ndph knockout mice correlate with high expression of Norrin and Frizzled-4. Eur J Neurosci. 2008; 27:2619–2628. [PubMed: 18547247]
54. Ye X, Smallwood P, Nathans J. Expression of the Norrie disease gene (Ndp) in developing and adult mouse eye, ear, and brain. Gene Expr Patterns. 2011; 11:151–155. [PubMed: 21055480]
55. Zhang Y, et al. An RNA-sequencing transcriptome and splicing database of glia, neurons, and vascular cells of the cerebral cortex. J Neurosci. 2014; 34:11929–11947. [PubMed: 25186741]
56. Nitta T, et al. Size-selective loosening of the blood-brain barrier in claudin-5- deficient mice. J Cell Biol. 2003; 161:653–660. [PubMed: 12743111]
57. Chen ZL, et al. Ablation of astrocytic laminin impairs vascular smooth muscle cell function and leads to hemorrhagic stroke. J Cell Biol. 2013; 202:381–395. [PubMed: 23857767]
58. Gould DB, et al. Mutations in Col4a1 cause perinatal cerebral hemorrhage and porencephaly. Science. 2005; 308:1167–1171. [PubMed: 15905400]
59. Winkler EA, Bell RD, Zlokovic BV. Central nervous system pericytes in health and disease. Nat Neurosci. 2011; 14:1398–1405. [PubMed: 22030551]
60. Winkler EA, et al. GLUT1 reductions exacerbate Alzheimer's disease vasculoneuronal dysfunction and degeneration. Nat Neurosci. 2015; 18:521–530. [PubMed: 25730668]
61. Ventura A, et al. Restoration of p53 function leads to tumour regression in vivo. Nature. 2007; 445:661–665. [PubMed: 17251932]
62. Maretto S, et al. Mapping Wnt/β-catenin signaling during mouse development and in colorectal tumors. Proc Natl Acad Sci USA. 2003; 100:3299–3304. [PubMed: 12626757]
63. Kuo CJ, et al. Comparative evaluation of the antitumor activity of antiangiogenic proteins delivered by gene transfer. Proc Natl Acad Sci USA. 2001; 98:4605–4610. [PubMed: 11274374]
64. Beck AH, et al. 3′-end sequencing for expression quantification (3SEQ) from archival tumor samples. PLoS One. 2010; 5:e8768. [PubMed: 20098735]

Author Manuscript Author Manuscript Author Manuscript Author Manuscript

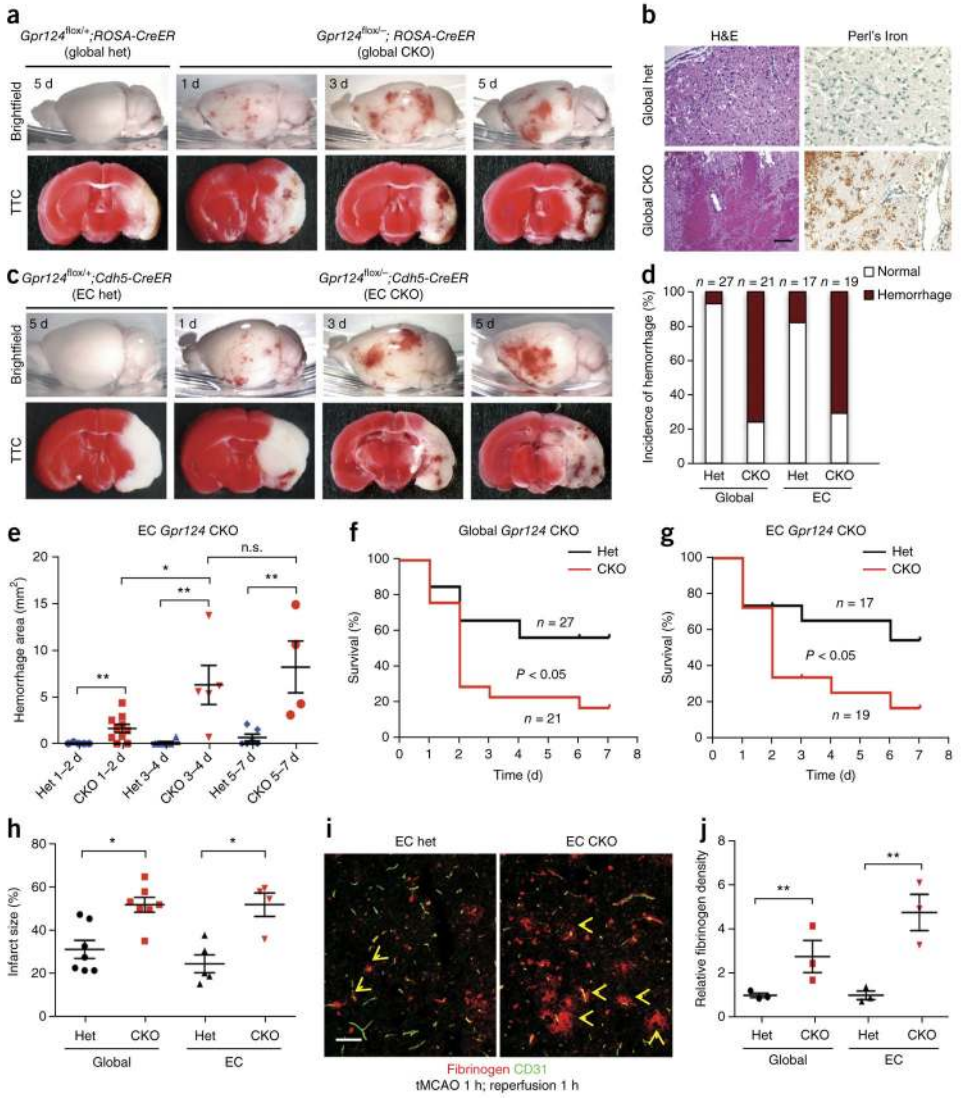

Figure 1.

Endothelial Gpr124 deficiency induces rapid BBB breakdown and hemorrhagic transformation following brain ischemia and reperfusion. (**a**) Gross appearance (top) and TTC staining (bottom) of brains of global *Gpr124*-CKO and het mice after 1 h tMCAO and 1–5 d reperfusion; intracerebral hemorrhage and infarcted areas (white in TTC staining) can be visualized. (**b**) H&E histological analysis (left) and Perl's Iron staining for red blood cells (right) to visualize microvascular hemorrhage. Scale bar, 100 μm. (**c**) Gross appearance (top) and TTC staining (bottom) of endothelial (EC) *Gpr124*-CKO and het mice after 1 h tMCAO and 1–5 d reperfusion. (**d**) The percentage of male mice of the indicated genotypes showing hemorrhage poststroke within 7 d reperfusion. (**e**) Quantification of hemorrhage area on the surface of the cortex and inside infarcted tissue of EC *Gpr124*-CKO mice and het mice after 1 h tMCAO and 1–7 d reperfusion. Het 1–2 d, $n = 5$ mice; CKO 1–2 d, $n = 10$; het 3–4 d, $n = 4$; CKO 3–4 d, $n = 5$; het 5–7 d, $n = 8$; CKO 5–7 d, $n = 4$. n.s., not significant, $^{*}P < 0.05$, $^{**}P < 0.01$, unpaired Student's *t*-test. (**f**,**g**) Survival of male global *Gpr124*-CKO mice (**f**) or

Author Manuscript Author Manuscript Author Manuscript Author Manuscript

EC *Gpr124*-CKO mice (**g**), together with their respective het controls, after 1 h tMCAO and 7 d reperfusion. $P < 0.05$, log–rank test. (**h**) Quantification of infarct size determined by TTC staining of male global *Gpr124*-CKO mice or EC *Gpr124*-CKO mice, together with their respective het controls. Global *Gpr124* het mice, $n = 7$; global *Gpr124* CKO, $n = 7$; EC *Gpr124* het, $n = 5$; EC *Gpr124* CKO, $n = 4$. $^{*}P < 0.05$, $^{**}P < 0.01$, unpaired Student's *t*-test. (**i**) Immunofluorescence staining of leaked endogenous plasma fibrinogen after 1 h tMCAO and 1 h reperfusion in EC *Gpr124*-CKO mice and het mice. Arrows point to plasma fibrinogen that has leaked out of vessels. Scale bar, 50 μm. (**j**) Quantification of plasma fibrinogen leakage in (**i**). Data are mean ± s.e.m., $n = 3$ mice per group. $^{**}P < 0.01$, unpaired Student's *t*-test.

Author Manuscript Author Manuscript Author Manuscript Author Manuscript

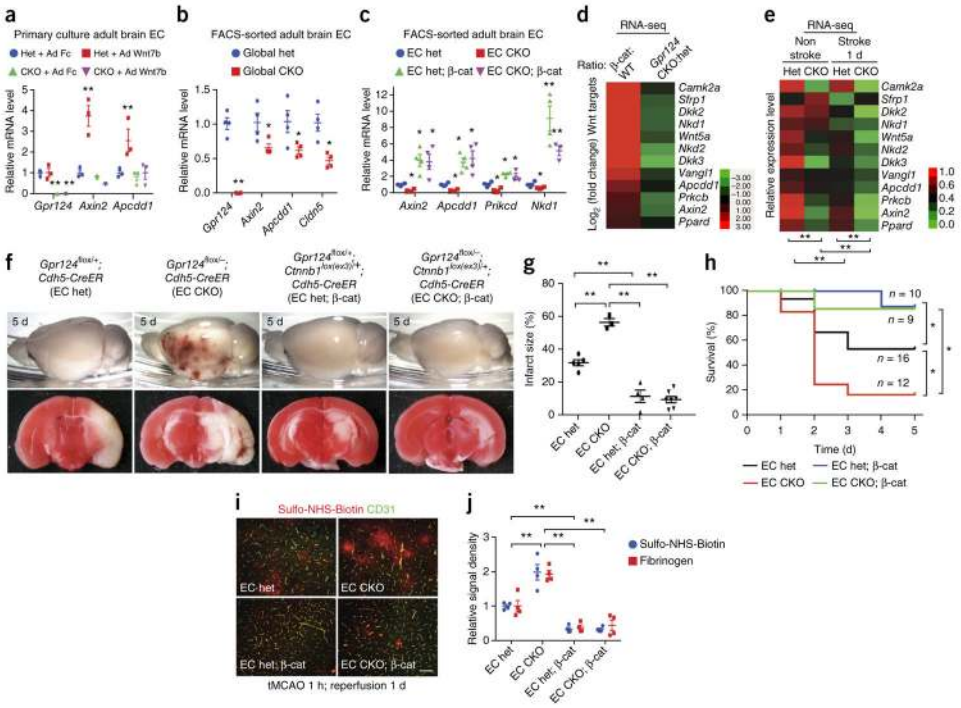

Figure 2.

Activation of endothelial Wnt–β-catenin signaling rescues the hemorrhagic-stroke phenotype of Gpr124-deficient mice. (**a**) Expression of *Gpr124* and the Wnt target genes *Axin2* and Apcdd1, as assessed by RT–qPCR, in primary brain ECs from adult global *Gpr124*-CKO and het mice; cells were infected with adenovirus expressing mouse IgG2α Fc (Ad Fc) or Wnt7b (Ad Wnt7b) for 2 d before determination of mRNA levels. Data are mean ± s.e.m. of triplicate experiments. $^{**}P < 0.01$, unpaired Student's *t*-test. (**b**) Expression of *Gpr124*, Wnt target genes and the BBB marker *Cldn5,* as assessed by RT–qPCR, in freshly isolated brain ECs of tamoxifen-treated global *Gpr124*-CKO mice versus het mice. Mean ± s.e.m., $n = 4$ mice per group. Individual mice are plotted. $^{*}P < 0.05$, $^{**}P < 0.01$, unpaired Student's *t*-test. (**c**) Expression of Wnt-signaling target genes, as assessed by RT–qPCR, in FACS-sorted adult brain ECs from EC *Gpr124*-CKO versus het mice with or without constitutive β-catenin activation (β-cat). Mean ± s.e.m., $n = 4$ mice per group. Individual mice are plotted. This experiment was repeated with $n = 4$ mice per group. $^{*}P < 0.05$, $^{**}P < 0.01$ versus het, unpaired Student's *t*-test. (**d**) Fold changes ($\log^2$) in expression of canonical Wnt-signaling target genes, as assessed by RNA-seq analysis, in FACS-sorted brain ECs from tamoxifen-treated mice, showing comparisons between *Ctnnb1$^{lox(ex3)/+}$;Cdh5-CreER* (β-cat) mice versus *Ctnnb1$^{+/+}$;Cdh5-CreER* (WT) mice ($n = 3$ mice per group), and global *Gpr124*-CKO mice versus het mice ($n = 4$ mice per group). (**e**) Relative expression levels of Wnt target genes, as assessed by RNA-seq analysis, of brain ECs from the stroke and nonstroke hemispheres of adult global *Gpr124*-CKO and het mice after 1 h tMCAO and 1 d reperfusion. For each gene, the level of gene expression is presented relative to the het nonstroke value and assigned to values between 0 and 1 to allow red–green color depiction. $n = 4$ mice per group. $^{**}P < 0.01$, paired Student's *t*-test. (**f**) Gross appearance (top) and TTC staining (bottom) of brains of EC *Gpr124*-CKO versus het mice with or without

Author Manuscript Author Manuscript Author Manuscript Author Manuscript

endothelial constitutive β-catenin activation to show intracerebral hemorrhage and infarcted areas (white in TTC staining) after 1 h tMCAO and 5 d reperfusion. (**g**) Quantification of infarct size determined by TTC staining. EC het, $n = 5$ mice; EC CKO, $n = 3$; EC het; β-cat, $n = 4$; EC CKO; β-cat, $n = 7$. $^{**}P < 0.01$, unpaired Student's *t*-test. (**h**) Survival of EC *Gpr124*-CKO versus het mice with or without endothelial constitutive β-catenin activation after 1 h tMCAO and 5 d reperfusion. $^{*}P < 0.05$, log–rank test. (**i**) Representative images of BBB integrity in brains of the indicated mice after 1 h tMCAO and 1 d reperfusion, as assessed by the Sulfo-NHS-biotin tracer extravasation assay. Scale bar, 50 μm. (**j**) Quantification of extravasated exogenous tracer Sulfo-NHS-biotin or endogenous plasma fibrinogen. Biotin or fibrinogen signal density was measured with ImageJ and normalized to vessel area (CD31). Data are mean ± s.e.m., $n = 4$ mice per group. $^{**}P < 0.01$, unpaired Student's *t*-test.

Author Manuscript Author Manuscript Author Manuscript Author Manuscript

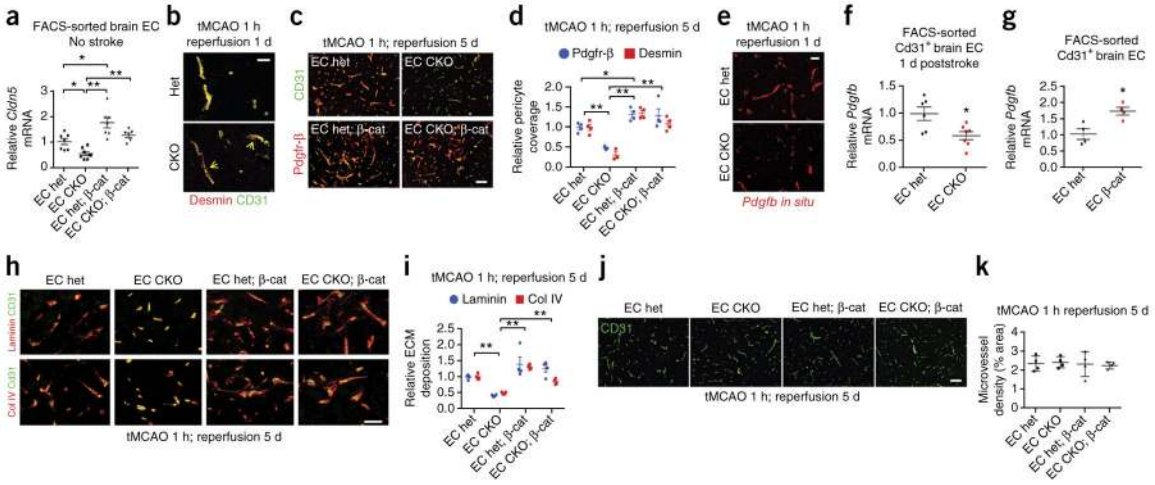

Figure 3.

Gpr124–Wnt signaling regulates endothelial tight junction, pericyte and extracellular matrix following stroke. (**a**) Expression of *Cldn5* mRNA, as assessed by RT–qPCR, using FACS-sorted adult brain CD31$^+$ ECs from EC *Gpr124* CKO versus het mice, with or without constitutive β-catenin activation (β-cat). Data are mean ± s.e.m., EC het, $n = 7$ mice; EC CKO, $n = 8$; EC het; β-cat, $n = 7$; EC CKO; β-cat, $n = 6$. Individual mice are plotted. $^*P < 0.05$, $^{**}P < 0.01$, unpaired Student's *t*-test. (**b**) Co-immunofluorescence staining for CD31 and desmin in infarcted brain regions after 1 h tMCAO and 1 d reperfusion of global *Gpr124*-CKO versus het mice. Arrows show desmin$^+$ pericytes detached from CD31$^+$ endothelial cells. Scale bar, 20 μm. (**c**,**d**) Co-immunofluorescence staining for Pdgfr-β and CD31 in infarcted brain regions (**c**) and quantification of pericyte coverage (**d**) after 1 h tMCAO and 5 d reperfusion in EC *Gpr124* CKO versus het mice with or without constitutive β-catenin activation. The lengths of Pdgfr-β or desmin staining signal surface were normalized to that for CD31; 6–8 low-power fields per mouse, EC het, $n = 4$; EC CKO, $n = 3$; EC het; β-cat, $n = 4$; EC CKO; β-cat, $n = 4$. $^*P < 0.05$, $^{**}P < 0.01$, unpaired Student's *t*-test. Scale bar in **c**, 100 μm. (**e**) *Pdgfb* expression, as assessed by *in situ* hybridization, in infarcted brain cortex of EC *Gpr124*-CKO mice and het controls after 1 h tMCAO and 1 d reperfusion. Representative images are shown from three mice. (**f**) Expression of *Pdgfb*, as assessed by RT–qPCR, in adult brain ECs from EC *Gpr124* CKO versus het mice after 1 h tMCAO and 1 d reperfusion. Infarcted brain tissues from two mice were pooled to form one sample; EC het, $n = 6$, EC CKO, $n = 7$. Individual mice are plotted. $^*P < 0.05$ versus EC het, unpaired Student's *t*-test. (**g**) Expression of *Pdgfb*, as assessed by RT–qPCR, in adult brain ECs from mice with EC *Gpr124*-het mice with or without constitutive β-catenin activation (EC β-cat). Data are mean ± s.e.m.; $n = 4$ mice per group. $^*P < 0.05$, unpaired Student's *t*-test. (**h**,**i**) Co-immunofluorescence staining for laminin and CD31 and for collagen IV (col IV) and CD31 in infarcted brain regions (**h**) and quantification of ECM protein levels (**i**) after 1 h tMCAO and 5 d reperfusion. Laminin and col IV signal densities were normalized to CD31 signal area. 6–8 low-power fields per mouse were randomly selected. Data are mean ± s.e.m., $n = 4$ mice per group. $^{**}P < 0.01$, unpaired Student's *t*-test. Scale bar in **h**, 100 μm. (**j**) CD31 staining in infarcted brain cortex in EC *Gpr124*-CKO versus het mice with or without constitutive β-catenin activation after 1 h tMCAO and 5 d reperfusion. Scale

bar, 100 μm. (**k**) Quantification of microvessel density, as assessed by the percentage of CD31 signal area to brain tissue area in (**j**). Five or six low-power fields per mouse were randomly selected. Data are mean ± s.e.m., $n = 4$ mice per group. Individual mice are plotted.

Author Manuscript Author Manuscript Author Manuscript Author Manuscript

Author Manuscript Author Manuscript Author Manuscript Author Manuscript

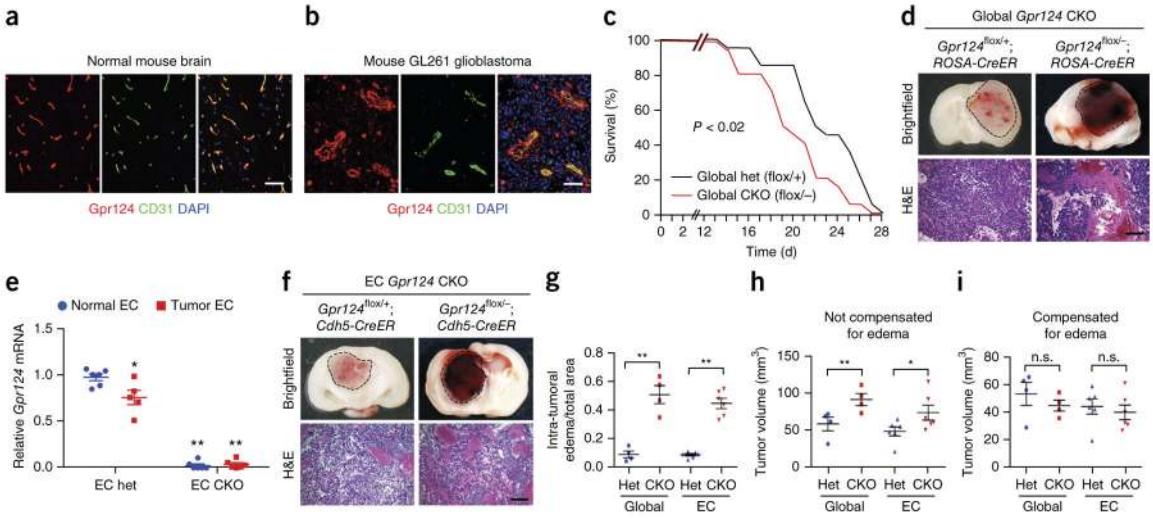

Figure 4.

Endothelial Gpr124 deficiency increases tumor hemorrhage and reduces survival in experimental glioblastoma. (**a**,**b**) Co-immunofluorescence staining for Gpr124 and CD31 in mouse normal brain tissue (**a**) and GL261 glioblastoma (**b**). The images are representative of those obtained from five mice. Scale bar, 100 μm. (**c**) Survival of global *Gpr124*-CKO and het control mice with implanted GL261 glioblastoma cells. $n = 15$ mice per group. $P < 0.02$, log–rank test. (**d**) Gross appearance and H&E histology of brain tumors in global *Gpr124*-CKO and het control mice. Representative images from 15–20 tumors are shown. Scale bar, 100 μm. (**e**) Expression of *Gpr124*, as assessed by RT–qPCR, in FACS-sorted $CD31^+$ ECs from normal brain and tumor tissue of EC *Gpr124*-CKO and het mice. $n = 6$ samples for EC het-normal, EC CKO-normal and EC CKO-tumor, and $n = 5$ samples for EC het-tumor; each sample consisted of FACS-sorted $CD31^+$ ECs from pooled normal or tumor tissue from two mice of the same genotype. Data are mean ± s.e.m., $^*P < 0.05$, $^{**}P < 0.01$ versus EC het-normal, unpaired Student's *t*-test. (**f**) Gross appearance and H&E analysis of brain tumors from EC *Gpr124*-CKO mice versus het controls. Representative images from 15–20 tumors are shown. Scale bar, 100 μm. (**g**) Intratumoral edema, quantified as the area of interstitial space within tumors absent of tumor cells but instead filled with blood cells or plasma, relative to total tumor area. Global *Gpr124* het, $n = 4$; global *Gpr124* CKO, $n = 4$; EC *Gpr124* het, $n = 6$; EC *Gpr124* CKO, $n = 6$. $^{**}P < 0.01$, unpaired Student's *t*-test. (**h**,**i**) Quantification of tumor volumes without (**h**) and with (**i**) compensation for edema. Global *Gpr124* het, $n = 4$; global *Gpr124* CKO, $n = 4$; EC *Gpr124* het, $n = 6$; EC *Gpr124* CKO, $n = 6$. Data are mean ± s.e.m. Individual mice are plotted. n.s., not significant, $^*P < 0.05$, $^{**}P < 0.01$, unpaired Student's *t*-test.

Author Manuscript Author Manuscript Author Manuscript Author Manuscript

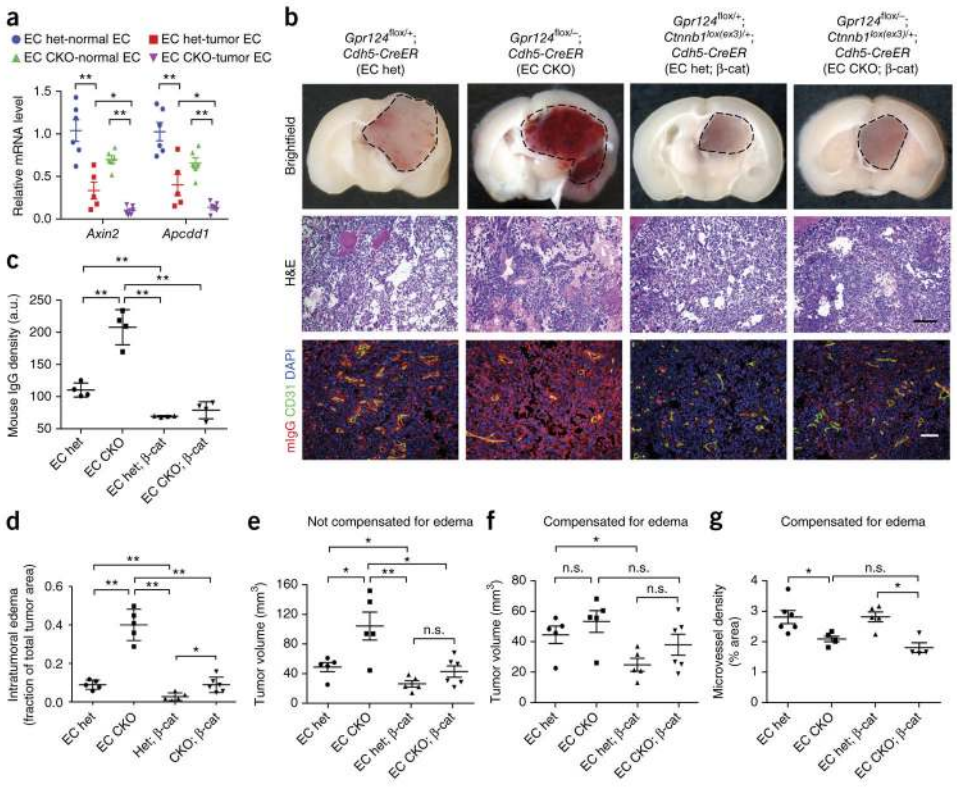

Figure 5.

Endothelial activation of Wnt–β-catenin signaling reduces tumor hemorrhage and edema in endothelial-specific *Gpr124*-deleted mice with glioblastoma. (**a**) Expression of Wnt-signaling target genes *Axin2* and *Apcdd1*, as assessed by RT–qPCR, in FACS-sorted CD31$^+$ ECs from normal brain and tumor tissue of EC *Gpr124*-CKO and het mice. $n = 6$ samples for EC het-normal, EC CKO-normal, EC CKO-tumor and $n = 5$ samples for EC het-tumor; each sample was FACS-sorted CD31$^+$ ECs from pooled normal or tumor tissue from two mice of the same genotype. Data are mean ± s.e.m., $*P < 0.05$, $**P < 0.01$, unpaired Student's *t*-test. (**b**) Gross appearance, H&E histology and co-immunofluorescence staining of mouse IgG (mIgG) and CD31 of brain tumors in EC *Gpr124*-CKO versus het mice with or without constitutive β-catenin activation. EC het, $n = 8$; EC CKO, $n = 6$; EC het; β-cat, $n = 6$; EC CKO; β-cat, $n = 6$. Representative images are shown. Scale bar, 100 μm. (**c**) Quantification of mouse IgG signal density relative to that of CD31 signal in **b**. Five or six low-power fields per mouse were randomly selected. a.u, arbitrary unit. $n = 4$ mice per group. Data are mean ± s.e.m., $**P < 0.01$, unpaired Student's *t*-test. (**d**) Intratumoral edema, quantified as the area of interstitial space within tumors absent of tumor cells but instead filled with blood cells or plasma, relative to total tumor area. EC het, $n = 5$; EC CKO, $n = 5$; EC het; β-cat, $n = 5$; EC CKO; β-cat, $n = 6$. $*P < 0.05$, $**P < 0.01$, unpaired Student's *t*-test. (**e**,**f**) Quantification of tumor volumes in EC *Gpr124* CKO versus het mice with or without constitutive β-catenin activation without (**e**) or with compensation (**f**) for edema. EC het, $n = 5$; EC CKO, $n = 5$; EC het; β-cat, $n = 5$; EC CKO; β-cat, $n = 6$. (**g**) Tumor-vessel density, quantified as CD31-positive signal area relative to tumor tissue area, with correction for edema. 6–8 low-power fields per mouse were randomly selected. EC het,

Author Manuscript Author Manuscript Author Manuscript Author Manuscript

$n = 6$; EC CKO, $n = 5$; EC het; β-cat, $n = 5$; EC CKO; β-cat, $n = 4$. *$P < 0.05$, unpaired Student's t-test. Data are mean ± s.e.m.

Author Manuscript Author Manuscript Author Manuscript Author Manuscript

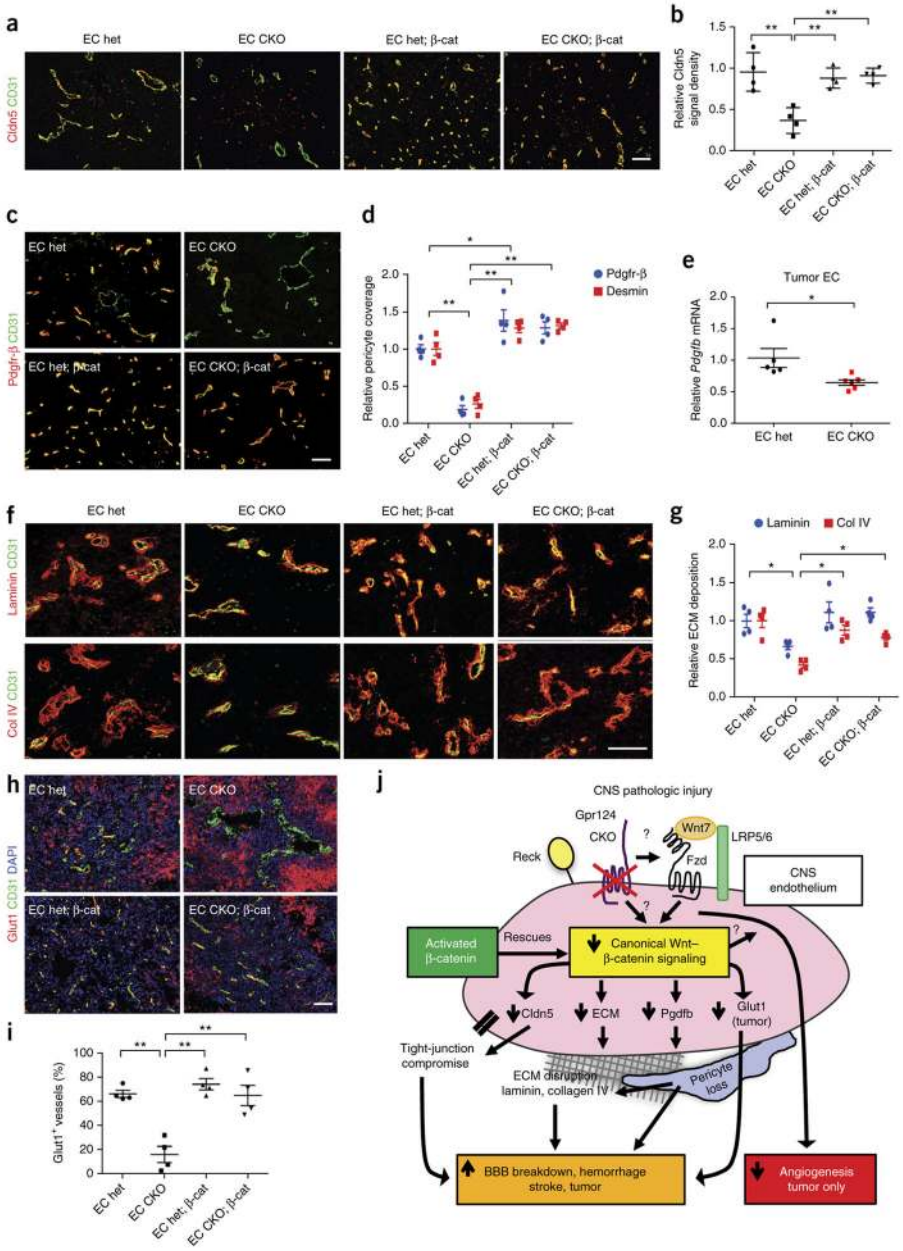

Figure 6.

Gpr124–Wnt signaling increases BBB integrity in glioblastoma by regulating tight-junction protein, pericyte coverage, Glut1 and the ECM. (**a**) Co-immunofluorescence staining for Cldn5 and CD31 in tumors of GL261-implanted EC *Gpr124* CKO versus het mice with or without constitutive β-catenin activation. Scale bar, 100 μm. (**b**) Quantification of Cldn5 signal density in (**a**) normalized to CD31 signal area. 6–8 low-power fields per tumor were randomly selected. $n = 4$ mice per group. Data are mean ± s.e.m. $^{**}P < 0.01$, unpaired Student's *t*-test. (**c**,**d**) Co-immunofluorescence staining for Pdgfr-β and CD31 of tumors (**c**) and quantification of pericyte coverage (Pdgfr-β^+ and desmin$^+$, **d**) in endothelial *Gpr124* CKO versus het mice with or without constitutive β-catenin activation. Pdgfr-β and desmin

Author Manuscript Author Manuscript Author Manuscript Author Manuscript

signal areas were normalized to CD31 signal area. 6–8 low-power fields per mouse were randomly selected. $n = 4$ mice per group. $^{*}P < 0.05$, $^{**}P < 0.01$, unpaired Student's *t*-test. (**e**) Expression of *Pdgfb*, as assessed by RT–qPCR, in FACS-sorted brain tumor ECs from EC *Gpr124*-CKO and het mice. $n = 5$ samples for EC het, $n = 6$ samples for EC CKO; tumor tissues from two mice were pooled as one sample. Data are mean ± s.e.m. $^{*}P < 0.05$, unpaired Student's *t*-test. (**f**,**g**) Co-immunofluorescence staining for laminin and CD31 and for collagen IV (col IV) and CD31 in tumor regions (**f**) and quantification of ECM protein abundance (**g**). Laminin and col-IV signal densities were normalized to CD31 signal area. 6–8 low-power fields per mouse were randomly selected. $n = 4$ mice per group. $^{*}P < 0.05$, unpaired Student's *t*-test. (**h**) Co-immunofluorescence staining for Glut1 and CD31 in tumors of EC *Gpr124*-CKO versus het mice with or without constitutive β-catenin activation. Note the strong expression of Glut1 in tumor cells in both *Gpr124* het and CKO tumors. Scale bar, 100 μm. (**i**) Quantification of the number of $Glut1^{+}$ tumor vessels. 100–200 vessels were counted per tumor. $n = 4$ mice per group. Data are mean ± s.e.m. $^{**}P < 0.01$, unpaired Student's *t*-test. (**j**) Schematic diagram illustrating the mechanisms underlying pathologic BBB breakdown and hemorrhage caused by Gpr124 deficiency. In ischemic stroke or glioblastoma, endothelial Gpr124 deficiency reduces Wnt7-dependent canonical β-catenin signaling, resulting in β-catenin activation-reversible effects: loss of tight-junction protein (Cldn5) and *Pdgfb* expression, pericyte loss, ECM disruption (laminin, collagen IV) and downregulation of endothelial Glut1 expression (in the glioblastoma setting only). Gpr124 deletion impairs angiogenesis only in the GL261 GBM, but not in acute stroke setting.